University of Alberta

Wear Behavior of Flame Sprayed Nanostructured Titania Coatings

by

Navid Pourjavad

A thesis submitted to the Faculty of Graduate Studies and Research
in partial fulfillment of the requirements for the degree of

Master of Science

Department of Mechanical Engineering

To my beloved mother

for her endless love and support.

And in memory of my beloved grandmother

for teaching me the importance of learning.

"A reasonable probability is the only certainty".

Edgar Watson Howe

Abstract

Various pressures of compressed air were introduced into the flame spraying torch and the protective coatings of nanostructured and conventional titania (TiO_2) were deposited on low carbon steel substrates. Performance of the coatings was studied using scanning electron microscopy (SEM), hardness measurement, porosity measurement and the best coating was selected for further analyses. A Nanostructured and conventional samples were exposed to ASTM G65 and C633 standard tests and the outcome was analyzed using confocal and electron microscopy. A nanostructured coating was found to outperform the conventional counterpart due to the presence of a bimodal microstructure, which increases the plastic deformation and crack resistance of the ceramic. The nanostructured coating was analyzed using X-Ray diffraction (XRD) and eventually its crack propagation resistance was quantified. The coating was also tested in a highly corrosive H_2S environment and Energy-dispersive X-ray spectroscopy (EDX) verified its fair resistance against that environment.

Acknowledgements

At this time when I look back at the last few years of my life, all I can remember is people to whom I owe my sincere gratitude. These are the people who affected the way I see the world, the way I think and the way I behave. Each one of these individuals taught me something valuable in this journey and I am honored to thank them at this point.

It is my pleasure to begin by thanking my supervisor, Dr. André McDonald. This thesis would not have been possible without his help, knowledge, and guidance. Apart from numerous technical skills that I learned from him, I would like to thank André for the way he trusted the students and gave them the opportunity to take responsibility by letting them be in charge of their own projects. I not only learned science but fundamentals of professionalism when working under his supervision and I am thankful for all of these.

I would like to extend my sincere gratitude to Dr. Gary Fisher for his invaluable support and guidance and his role in defining the project that I worked on for my thesis. I also want to thank Dr. Adrian Gerlich for the useful discussions we had as well as for letting me use his lab for some parts of this study. It is my great pleasure to thank Dr. Jason Carey for chairing my defense session and providing me with so much helpful advice. It is an honor for me to have these gentlemen as my defense committee and I appreciate the time they spent on reading my thesis and providing me with their valuable comments.

I also want to gratefully acknowledge the help of Mr. Bernie Faulkner, Mr. Roger Marchand and Mr. Rick Conrad, specialist technicians in

Table of contents

List of tables

List of figures

Abbreviations

APS	Air Plasma Spray
ASTM	American Society for Testing and Materials
BSE	Back Scattered Electrons
EDX	Energy-Dispersive X-Ray spectroscopy
FMR	Flow Meter Reading
FS	Flame Spray
HV	Hardness Vickers
HVOF	High Velocity Oxy-Fuel spray
NLPM	Normal Liters per Minute
SCFH	Standard Cubic Feet per Hour
SD	Standard Deviation
SE	Secondary Electrons
SEM	Scanning Electron Microscopy
XRD	X-Ray Diffraction
YSZ	Yttria-Stabilized Zirconia

Chapter 1

Introduction

Background

Thermal spraying is a general name for a group of processes used to deposit coatings on a substrate from molten droplets. The coating material can be ceramic, metal or even polymer. These materials are fed into a flame in the form of a powder, wire or rod. The flame will melt and accelerate the feedstock toward the prepared substrate surface. The molten droplets strike the substrate surface one after each other and form the coating. The coating made by this method is lamellar and stratified, and the thickness of the coating can be controlled by increasing the number of layers deposited.

The torch which melts the material can be powered with different sources of energy. Based on the gun and coating material which is

used, thermal spraying can be divided into several categories, namely, plasma spraying, high velocity oxy-fuel (HVOF) spraying, flame spraying, and wire-arc spraying [1,2]. The source of power in plasma spraying is the electric arc which is produced by a plasma spray torch. In case of wire-arc spraying, the source of heat is the same electric arc but produced between the consumable rods or between one rod and a non-consumable cathode [3,4].

The HVOF and flame spraying processes use a mixture of oxygen and a hydrocarbon fuel. This fuel is usually propylene and acetylene, respectively. The combustion of these fuels in the torch provides the heat to melt and accelerate the droplets towards the substrate. The droplets then hit the surface of the substrate and solidify at impact. The solidified splats form the lamellar coating, layer by layer.

Thermal-sprayed coatings are used for a variety of applications. Some of the applications are to provide wear resistance, oxidation resistance, corrosion resistance, dimensional restoration, thermal barriers, electrical conductivity and resistivity. These coatings are recently considered to be used in biomedical applications as well [5].

Due to its low cost of equipment and operation, oxy-acetylene flame spraying is known as the lowest-cost process of all thermal spraying methods. The equipment is also much more portable than HVOF and plasma spraying equipment [2]. Figure 1 shows a schematic of the flame spraying process, where the powder particles are being melted by the torch and deposited on the substrate. In case of spraying the nanostructured titania feedstock The flame spraying process delivers the highest particle temperature while the HVOF spraying process delivers the lowest particle temperatures. On the other hand, the velocity of the flame-sprayed particles seems to be the least of all while this value is the highest at HVOF spraying. Air plasma spraying (APS) has the temperature and velocity values somewhere between the HVOF and flame spraying process [2]; however, this process is capable of producing the highest flame temperature of all.
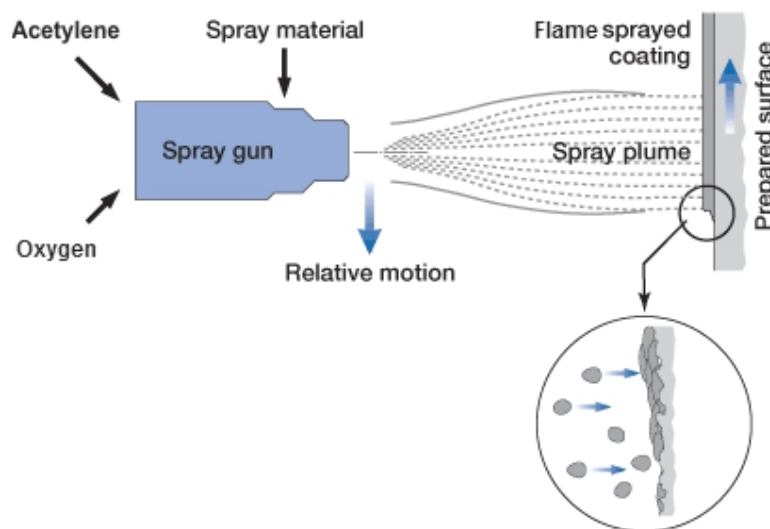
Figure 1: Schematic of flame spraying [6]

Thermal spray coatings are considered as one promising solution for anti-wear applications, specifically in situations where sliding wear and abrasive particles are present. Examples of these types of applications are the pump seals and bearing surfaces which can be coated by thermal-sprayed coatings for increasing their resistance [7,8].

Engineering parts are degraded by four major degradation processes: fracture, corrosion, wear and unwanted deformation [9]. Ceramic coatings have already proved to be good candidates for resistance against wear and corrosion [10]. Meanwhile there are several obstacles in the way of using ceramics in industry that can limit the usage of these engineering materials. Finding a solution for these problems can have a huge impact on application of ceramics. These problems are usually rooted in the mechanical properties of ceramics.

In general, ceramics tend to be very hard and stable in combating wear and corrosion. But, they usually present very low toughness values and they are generally brittle. The brittleness of ceramics sometimes prevents them from being used as engineering materials in places where plastic or severe elastic deformation is present. Recently,

thermally sprayed ceramic coatings fabricated from nanostructured powder particles have shown improved mechanical properties compared to coatings fabricated from conventional powders. Their plastic deformation, crack propagation resistance and toughness are also shown to be superior in comparison to the other counterparts [10]. Therefore this new kind of ceramics could be more effective when used as coating materials on the parts exposed to severe wear conditions.

Nanostructured powders are made by spray-drying process. In this process very fine-size nano powders are agglomerated into a larger-size particles which have the appropriate size to be used with thermal spraying equipments. The process starts with a slurry of the nanosized particles. The slurry is then injected into a counter-current stream of a cyclone of heated air. By vaporization of the liquid part, fine particles are agglomerated into donut-shape powder particles and can be collected at the bottom of the cyclone chamber [11,12]. These new powder particles are large enough to avoid clogging of the thermal spraying tubes and equipment.

While spraying these nanostructured powders, due to their high traveling speed in the thermal spray flame, complete melting might not happen in some the powder particles. The unmolten or semi-molten

nanostructured particles (Fig. 2) will then be present in the thermally sprayed coating and the resulting microstructure will affect the mechanical properties of the coating in different ways such as arresting the cracks propagating through the splats and inter-splat spaces [2].
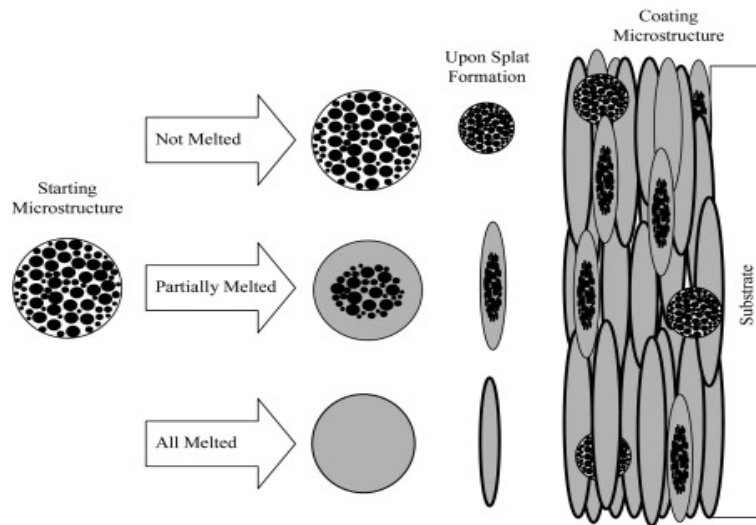
Figure 2: Schematic view of nano particles being deposited in thermal spraying [13]

Wear in engineering materials can be divided into two major categories: Abrasive wear and Adhesive wear. The abrasive wear is the dominant phenomenon in ceramic materials. Three different mechanisms of material removal between abrasive material and the surface have been observed and mentioned in literature. These three are: plowing, cutting and fragmentation (Fig. 3).

Plowing happens when the material is displaced to the side by the abrasive particle; the ridges that occur are removed afterwards. Cutting happens when the materials are removed in the form of micro chips and debris, like the machining process, and fragmentation occurs when the material is cut from the surface and the localized cracks propagate and result in more removal of the surface material [9].

Microplowing

Microcutting
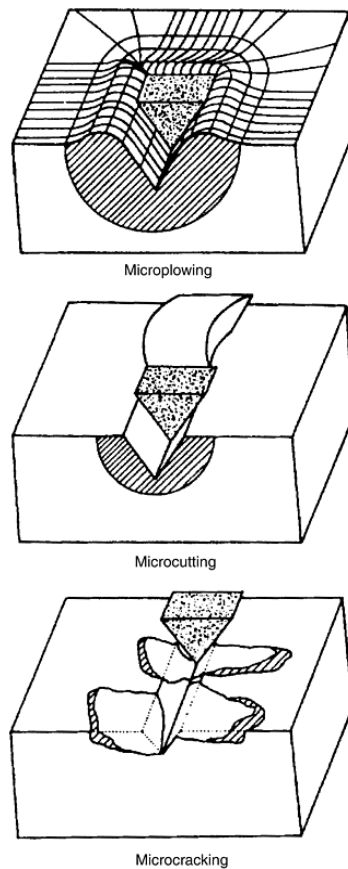
Microcracking

Figure 3: Microscopic mechanisms of material removal at abrasive wear [9]

Microplowing and microcutting involve plastic deformation, but microcracking is completely dominated by brittle fracture. Materials with high crack resistance and low yield strength are prone to be worn away by plowing. On the other hand, less ductile materials with higher values of yield strength are likely to be abraded by the fragmentation mechanisms. Ceramics which are considered to be hard materials with no ductility are supposed to behave like the third group and microcracking is supposed to be the main material removal process in them. [14-16].

From a macroscopic perspective abrasive wear can be classified into the following groups: Gouging abrasion, Hi-stress or grinding abrasion, Low stress or scratching abrasion and Erosion-corrosion. Among these, the low stress abrasion wear or scratching is the dominant form of wear in the pumping of sand slurries. Ceramics and ferrous alloys with hard carbide particle embedment are some of the best options to combat this kind of wear mechanism [9].

In order to use thermal spray titania coatings in industry, it is important to know about their capabilities. In the present document several mechanical properties of nanostructured titania are going to be investigated and analyzed.

Previous studies

Nanostructured coatings have been studied by different researchers. Most of them focused their research on plasma sprayed or High velocity oxy-fuel sprayed coatings. Nano powders were commercially available to researchers by the late 1990s. In 1997 Dr. Lawrence T. Kabacoff at the United States office of naval research began a program called "Thermal Spray Processing of Nanostructured Coatings" which was the start of using nanostructured ceramics as wear resistant materials [17,18]. The refereed journal articles about the nanostructured thermal spray coatings began to be published from the year 2000. Since then researchers are studying different aspects of thermal spraying and opening new horizons in this field [8].

A number of researchers studied the toughness of the nanostructured thermally sprayed ceramic coatings and they related this behaviour to the bimodal structure shown in Fig. 2. The wear resistance of the coatings was also assumed to be related to the toughness of the coating material [13,19]. Others studied the hardness values of the nanostructured coatings. It was generally believed that for the ceramic oxide thermal spray coatings the hardness of the coatings is the most important factor in its anti-wear performance. But, researchers working on Air Plasma Spraying (APS) of Al_2O_3-13 wt% TiO_2 showed

that apart from the higher Vickers hardness values of the conventional coatings, the nanostructured ones exhibited improved abrasion and sliding wear resistances [13,19-25]. Research on different thermally sprayed powder materials, such as TiO_2, YSZ and Al_2O_3- 3 wt.% TiO_2 also revealed a higher sliding and abrasion wear resistance of nanostructured coatings while the hardness values of both conventional and nanostructured coatings were at the same level [26-30]. It has also been observed that in cases like Al_2O_3, nanostructured coating shows both higher hardness and higher wear resistance than the conventional counterpart [10,31].

Crack propagation of ceramic coatings as a measure of toughness was another area that has also been studied by several researchers. Their observations report a significant enhancement in relative toughness and wear resistance of the nanostructured alumina-titania coatings when compared to the conventional ones. Most of these researchers used plasma spraying or HVOF spraying torches for their studies [13,14,16,18-20,22,24,26].

Development of wear resistant ceramic coatings has received particular attention by many researchers. Wear resistance of conventional and nanostructured coatings (sprayed via APS and HVOF

processes) were measured and compared. According to these studies, nanostructured TiO_2 performed 25% to 52% better than the conventional counterpart while tested for sliding wear performance and the volume loss was measured [26,27]. Nanostructured Al_2O_3 and Al_2O_3- 3wt% TiO_2 have also performed 39% and 32% better than their conventional coatings respectively [29,31]. Al_2O_3- 13wt% TiO_2 nanostructured coating has been shown to outperform the conventional one by 71%to 75% [22-24] and nanostructured YSZ's wear resistance increased from 21% to 75% in different studies as well [13,30,34-37].

Though many investigations have focused on characterizing the wear performance of APS and HVOF-sprayed coatings, few researchers have focused their attention on the wear performance of coatings fabricated by the flame spraying process. Moreover all of these studies targeted the sliding wear behaviours of flame sprayed titania coatings. Thus there seems to be a need for investigating the abrasion wear behaviour of nanostructured titania coatings further.

Lima and Marple [26] studied HVOF-sprayed nanostructured titania (TiO_2) and they have compared it to the conventional counterpart. They noticed a uniformly dispersed bimodal structure throughout the nanostructured coating. They also found out that despite the

equivalent hardness of nanostructured and conventional titania coatings, the nanostructured one has a 65% higher fracture toughness. The nanostructured coating proved to have 2.4 times stronger equivalent bond strength between the coating and the substrate (ASTM C633) and had 25 percent less average volume loss than the conventional coating during the abrasion wear test. These were indications of enhanced ductility due to the presence of semi molten particles in the coating and they were hypothesized to be related to the nanostructured properties of titania [26].

Another study of the flame sprayed nanostructured titania along with the HVOF and APS titania coating was done by Lima *et al.* [2]. They also used different titania powders i.e. fused and crushed and plasma fused titania powder and compared the sprayed coatings to the nanostructured one. They have found that the flame sprayed titania made from the nanostructured powder to be the best option in combating sliding wear. Negligible volume loss were observed during the ball-on-disk dry sliding wear test for flame sprayed nanostructured titania while the coating made by fused and crushed powder had a volume loss equal to 5.06 mm^3. To study the effect of nanostructure on the wear behaviour, they compared HVOF sprayed titania made from nano powder to the plasma fused powder. The nanostructured coating

showed 12 times less volume loss than the plasma fused coating during the sliding wear test. The temperature and in-flight velocity profiles of different torches were also measured by Lima *et al.* [2]. The study showed that in case of particle velocity, HVOF has the fastest particles (896 ± 89 m/s) of all the three techniques while flame spraying has the slowest ones (70-80 m/s). On the other hand in case of particle in-flight temperature it was observed that the flame sprayed particles have the highest temperature of all (2750°-2850° Celsius) while the HVOF particle are the coldest ones with a temperature of 2072°± 187° Celsius. The APS process values were measured to be in between of these numbers at both cases.

Sliding wear resistance of conventional and nanostructured plasma sprayed Al_2O_3- 13wt% TiO_2 were studied by Ahn *et al.* [23]. They reported the crack initiation and propagation along the splat boundaries as the main reason for volume loss of conventional coating. They concluded that stronger inter-splat bonds play an important role in the wear resistance of these coatings. Their studies also revealed three to four times more sliding wear resistance in nanostructured samples. They also reported the wear debris as coarse and flattened in conventional coating and small and rough in nanostructured counterpart.

In a recent study, Bolelli *et al.* [38] investigated the wear behaviour of thermal sprayed coatings (Al_2O_3, Al_2O_3-13%TiO_2 and Cr_2O_3) and linked this wear resistance to the inter-splat chemical and mechanical bonding in ceramics. The high melting point of some ceramics were said to be the reason for rapid solidification and not giving enough time to underlying splats to reach temperatures high enough for a good inter-splat bonding. They found thermal spray ceramic coatings to be the best at resisting wear, especially in lower revolutions of standard abrasion wear test wheel. They also described brittle fracture and inter-splat crack propagation as the main relevant wear mechanism in thermally sprayed ceramics which do not undergo plastic deformation phenomena like micro cutting and micro plowing. They also discussed the fact that fracture toughness (K_C) of the ceramic coatings, is not a parameter which is sufficient to describe the wear resistance of the coatings.

An equation was developed by Berger-Keller *et al.* [39] which made it possible to measure the percentage of nanozones by comparing the intensities of the X-Ray Diffraction (XRD) peaks for [1 0 1] reflection of anatase and [1 1 0] reflection of rutile. The equation was based on the fact that the anatase powder turns into rutile when melted and

resolidified during the spray process. The transformation of anatase to rutile depends on impurities, grain size, reaction atmosphere and different other factors; however, for a particle size of smaller than 50nm anatase was found to be more stable and transformed to rutile at approximately 700 ºC [40]. Another research in this area reported that the transformation of rutile to anatase in low pressures happen in the temperature range of 600 to 700 ºC [41]. To date there is not enough data to hypothesize a relationship for the optimum amount of semi-molten particles to get the best mechanical performance of the coatings, in spite of this, some studies showed that APS nanostructured Al_2O_3- 13wt % TiO_2 performs best when the percentage of these nanozones are 15% to 20% [22] and 11% [23]. Also about the HVOF sprayed nanostructured TiO_2 the XRD showed that the concentration of the nano zones was approximately 25% for the best performance [13,19,22,24].

Kim *et al.* [18] studied the APS nanostructured titania coating and subjected it to ASTM G65 wear testing. The results revealed a 30% decrease in volume loss in nanostructured than the conventional APS titania coating in addition to an increase in the hardness value. In the same study it was reported that using specific spray parameters they

could produce nanostructured coating that performs almost 20 times better than the conventional counterpart.

In their most recent study, Gaona *et al.* [42] studied the HVOF sprayed nanostructured titania. Unlike the traditional lamellar structure of thermal spray coatings, no stratification in the coatings was observed in their case. They have used the DVP-2000 in-flight diagnostic tool to measure the in-flight temperature and velocity of the particles. It was found that the porosity of these coatings decreased when the particle in-flight temperature and velocity increased. Opposite behaviour was noticed in case of hardness and concentration of anatase phase in the coating which had increasing trends. The data for the content of anatase in the coating was acquired using the Berger-Keller equation [39]. ASTM C633 testing was also done on the samples and the results revealed that the failure happened not across the interface but in the epoxy glue. Therefore the exact bond strength of the coatings could not be measured and it can only be stated that the bond strength is higher than the indicated value for the adhesive epoxy glue.

In the present document, flame sprayed nanostructured titania was studied and different mechanical properties of the coatings were investigated. Abrasion resistance of this coating is also going to be

targeted for investigation since there is a lack of data in literature around this subject.

Objectives

The objectives of this study are to:

- Determine the applicability of flame-sprayed nanostructured and conventional titania coatings under severe abrasive wear conditions.

- Analyze the wear mechanisms that occurred in the flame-sprayed nanostructured titania coating during service in abrasive wear conditions found in oil and gas industry.

- Use the surface topography analysis of the coatings to describe performance during wear applications.

- Run a preliminary H_2S corrosion test on the nanostructured coating to study its potential as an alternative coating to be used in combined abrasive and corrosive environments.

Thesis organization

Following the introduction in chapter 1, the second chapter of this thesis explains the setup and experimental procedures used to deposit and test the titania coatings. Results and discussion follows with summarizing the data acquired from scanning electron microscopy (SEM), confocal microscopy, hardness tests, porosity measurements, abrasion wear resistance test (ASTM G65), substrate-coating adhesion test (ASTM C633), roughness measurements, X-ray diffraction patterns and EDX mappings of H_2S corrosion test in chapter 3. Discussions of the presented results and hypotheses that justify the behaviour of the titania coatings under different testing conditions follow each specific topic as well as an investigation on differences between the nanostructured and conventional coatings in each case. Eventually a conclusion for this study is presented in the closing chapter.

Chapter 2

Experimental Procedure

Nanostructured coatings were deposited using flame spraying. Deposited coatings were then subjected to different tests and measurements. In the present chapter, each testing and fabrication method used, is mentioned and explained to the details.

Flame spray

Flame spraying is one of the several methods classified under the category of thermal spraying. This method is used to deposit coatings from ceramic, metallic and polymeric powders.

The setup used in this study included a flame spray torch (6P-II, Sulzer Metco, Westbury, NY, USA), attached to a Motoman robot arm

(HP20, Yaskawa Electric Corporation, Fukuoka, Japan) with a NX100 controller (Yaskawa Electric Corporation, Fukuoka, Japan) that can move the torch at different angles and with different speeds. The 6 axis robot was programmed in a way such that it moves the torch horizontally on a line that is three inches longer than the width of the substrate from each side. The torch moves up by 3mm increments until the entire surface of the substrate is covered with coating. To make sure that the torch does not miss any part of the surface, the program covers the entire height of the substrate plus one inch from each side. The speed of the torch is steady and it is equal to 400mm/sec while passing over the substrate. The torch burns a mixture of acetylene and oxygen to produce the flame for melting the powders. A Sulzer Metco 3GF flow meter (Westbury, NY, USA) is used to adjust the amount of acetylene and oxygen entering the torch. The exact flow of each gas is mentioned in table 1. Figs. 4 and 5 show a schematic and an actual photograph of the setup used in this study.

The powder is injected into the flame by a Sulzer Metco powder feed unit (5MPE, Westbury, NY, USA) which uses compressed air to mix the powder prior to injection. Argon is used as the primary gas and hydrogen is used as the secondary gas in this powder feeder only to pressurize the primary gas. The powder feed rate was adjusted to the

desired amount using this unit and the exact flow of the carrier gas (Argon) was set to 20 standard cubic feet per hour.
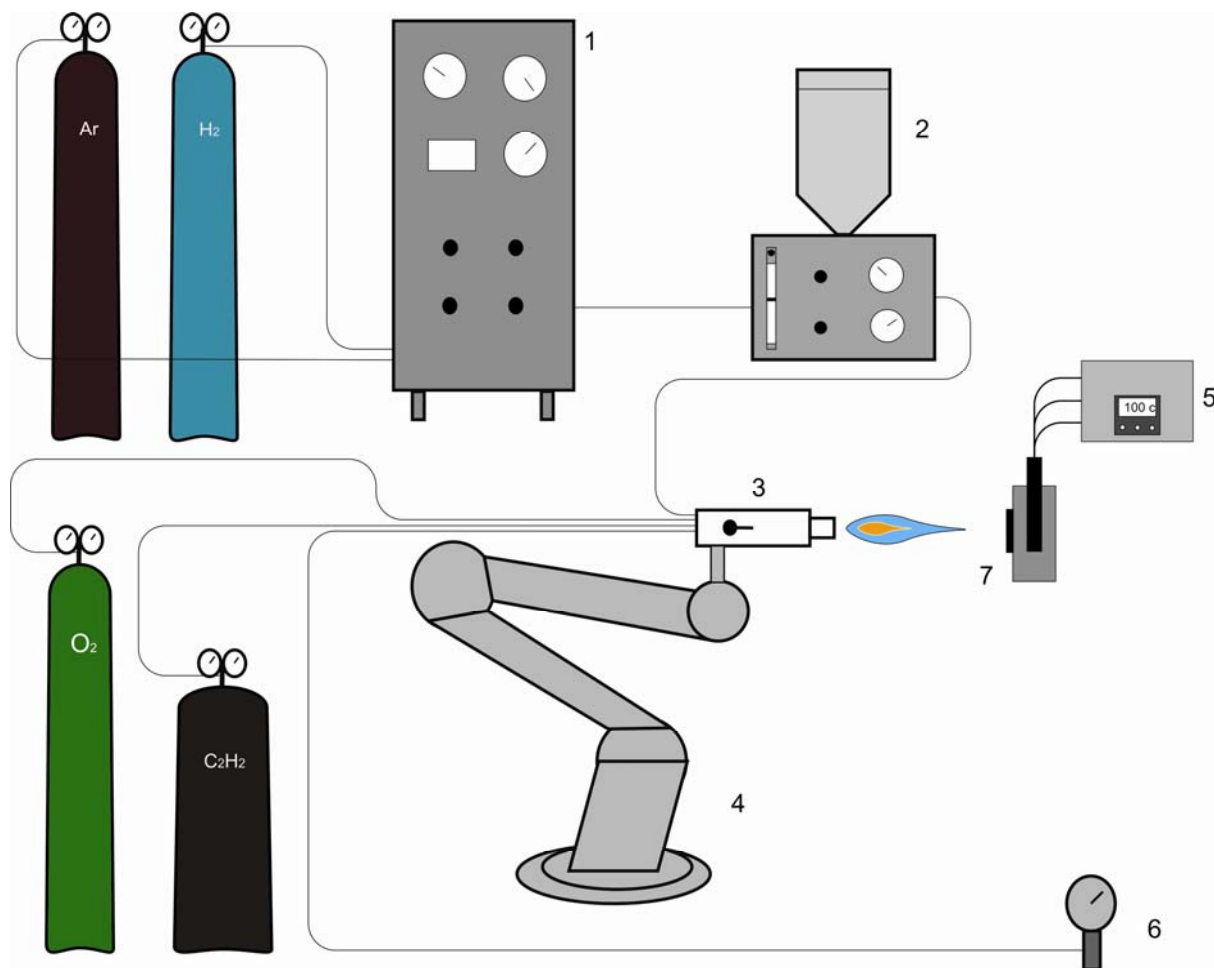
Figure 4: Schematic view of the flame spray setup. 1)9MC control unit 2)5MPE powder feed unit 3)6P-II flame spray torch 4)Motoman HP20 robot arm 5)Omega substrate heater 6)compressed air unit 7)Samples attached to the substrate holder and the heating cartridge(black) inside it

The torch is also fed by compressed air in order to speed up the particles toward the substrate as well as to decrease the temperature of the substrate by convection. The pressure of the compressed air entering the torch can be adjusted up to a maximum of 60 psi. A schematic view of the compressed air unit (6) attached to the torch (3) can be seen in Fig. 4.

The substrate was heated using a cartridge heater (iSeries CNi32, Omega, Stamford, CT, USA) that was installed within the substrate holder. The heater used electricity to preheat the substrate to an adjustable temperature. The feedback was measured using a K-type thermocouple attached to the substrate holder.
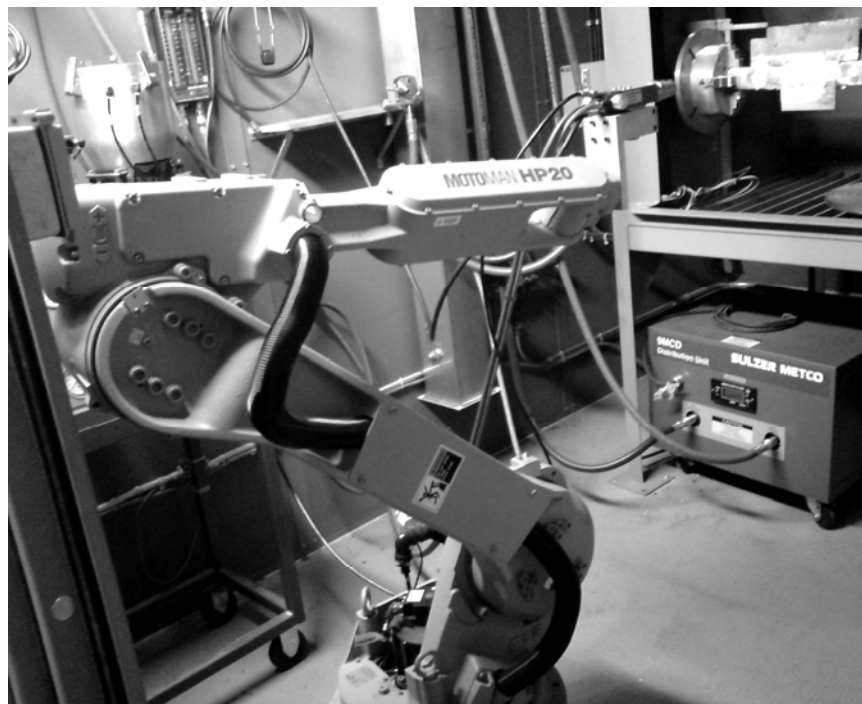
Figure 5: Photograph of the flame spray setup

The spray parameters which were used to deposit these coatings are summarized in Table 1. The only parameter that changed during the flame spaying of the coatings was the pressure of compressed air in the torch.

Table 1: Spray parameters used to deposit coatings

Powder feed rate	65 FMR (Flow Meter Reading)
Carrier gas flow rate	20 SCFH (Standard Cubic Feet per Hour)
Vibrating air pressure	70 psi
Torch stand-off distance	10 cm
Compressed air pressure	Variable(5-50 psi)
Acetylene flow rate	22 NLPM (Normal Liters per Minute)
Oxygen flow rate	35 NLPM (Normal Liters per Minute)
Torch speed	400 mm/sec
Number of passes	Variable
Increment	3 mm
Substrate	Conventional low carbon steel
Preheat	100 degrees Celsius

Powders and substrates

In flame spraying process, coating materials are deposited from a powder feedstock. In this study two different titania powders were

used to study the difference between the nanostructured coating and the conventional titania coating.

The nanostructured powder which was used to make the coatings was Altairnano TiCP2-P-01-050628-289 (Altair Nanotechnologies, Inc. Reno, NV, USA). Nanostructured coatings including this one are usually made by spray drying. As mentioned before spray drying is a process in which the nanosized particles are agglomerated to form larger sized powder particle that can then be used for thermal spraying.

The conventional titania powder, Metco 102 made by Sulzer Metco (Westbury, NY, USA) was used to deposit the conventional titania coating samples. Unlike the nanostructured one, this powder is made through fusing and crushing process. The titania powder which is made by this procedure is dark gray coloured; on the other hand the titania powder which has been made by spray drying is pale yellow. Difference of color is due to the prominent phase of titania that forms each powder. The majority of titania in nanostructured powder happens to be anatase, while rutile is the prominent titania phase present in conventional feedstock powders.

Both of these powders were sieved to a grain size distribution of smaller than 38 micrometers and larger than 20 micrometers to meet the requirements for the previous studies on this topic. The sieving was done by the standard Canadian standard sieve series (W.S. Tyler, St. Catherine, Ontario, Canada) and RO-Tap sieve shaker (Model: RX-29-CAN, W.S. Tyler Mentor, OH, USA) as shown in Fig. 6.

Figure 6: Sieving equipment

The substrate used in this study was conventional low carbon steel which was cut from a roll-milled plate with a thickness of half an inch. The substrates were cut in different sizes for the different tests. The samples for the ASTM G65 test were cut by a band saw and the standard size was 3 inches by 1 inch by ½ inch. Other samples were made for microscopy and hardness test the size was approximately ¾ inch by ½ inch by ½ inch. Samples for ASTM C633 test was made exactly according to the standard [43].

All of the substrates were grit blasted using #24 alumina grit prior to spraying. This surface preparation step was done to remove the oxides from the surface and clean the greasy parts as well as roughening the surface to a desired degree for the thermal spraying. During grit blasting, care was taken to avoid work hardening of the surface. The grit blasting was done with a stand-off distance of approximately 2 inches using a Trico dry blast (Fraser, MI, USA) instrument. After grit blasting, the surface was blasted with high pressure air to remove the remnants of grits from the surface.

Scanning electron microscopy and porosity measurement

Porosity is one important factor that affects the hardness of the ceramic coatings. To measure the porosity of the titania coatings, samples were mounted in resin or Bakelite and then cut and grinded using sand papers (Numbers: 240-400-800-1200) according to the conventional metallography process. After metallography and micro polishing of the samples, images from different points on the cross section of the samples were taken using scanning electron microscopy (SEM). Before microscopy the samples were carbon coated for conductivity. Secondary (SE) and back-scattered electron (BSE) images

were taken using a Zeiss SEM (Zeiss EVO MA 15, Carl Zeiss SMT Inc. North America). The pictures were cropped and the coating part was analyzed using Image-Pro Analyzer 6.3 (Media Cybernetics Inc. Bethesda, MD, USA) and the porosity of the samples was measured. The software measures the porosity by color difference and gives it as percentage of the examined area. In gray scale SEM images, a pore may be just a black spot or a combination of a black spot with a bright ring around it. To minimize the software error the black spots and the bright ring were selected manually by selecting a certain part of the color gradient of each image.

Indentation

Hardness plays an important role in the performance and quality of the ceramic coatings, therefore measuring it would give us valuable information about the coatings. The hardness was measured using a Vickers microhardness testing instrument (Model: MVK-H1, Mitutoyo, Buehler, Canada). The instrument was calibrated using a calibration metal disc with a known hardness value of 690 HV. The hardness measurements were done according to the ASTM C1327-08 standard test method for Vickers indentation hardness of advanced ceramics

[44]. The coating was placed under the indenter and the indentation was forged on the coating by a force of 200 grams and duration of 15 seconds. Then the indenter was removed and the diamond shape indentation was observed using the microscope. The diagonals of this diamond were measured and the hardness value was calculated by the instrument automatically from these diameters.

A similar procedure was used to measure the crack propagation resistance of the samples. The difference was the force load which was 1kg applied for 15 seconds in this case. Five indents were put on the polished cross section of each sample and the diamond shape indentations were imaged using all-in-focus confocal microscopy technique. The tip to tip crack length initiating from the edges was measured and analysed in the results section.

ASTM G65 standard test

In this study the coatings were subjected to different standard tests including ASTM G65 or the same "Standard test method for measuring abrasion using dry sand/rubber wheel apparatus" [45]. For this standard test, the low carbon steel samples are made in a standard

size (3 inches by 1 inch by ½ inch) and then coated by flame sprayed titania, these coatings are weighed and placed into the test assembly. The setup is consisted of an abrasive wheel, a sand hopper and a specimen holder which presses the specimen toward the wheel with a force of 130 N. Figure 7 shows a schematic view of the ASTM G65 test and how the samples are mounted on the instrument. More details and the exact specification of the instrument can be found in ASTM G65-04 standard document. When the specimen is fastened to the specimen holder, the wheel starts to turn and the hopper will feed the sand between the wheel and the specimen. The rubber-lined wheel then moves on the surface of the specimen and grinds the coating using the sand which is being fed continuously. The standard test is supposed to run for 6000 revolutions of the wheel, but in this study the revolutions were reduced to 250 due to the rigorousness of the test. The specimens are then taken out and weighed again, and the mass loss or volume loss is reported.
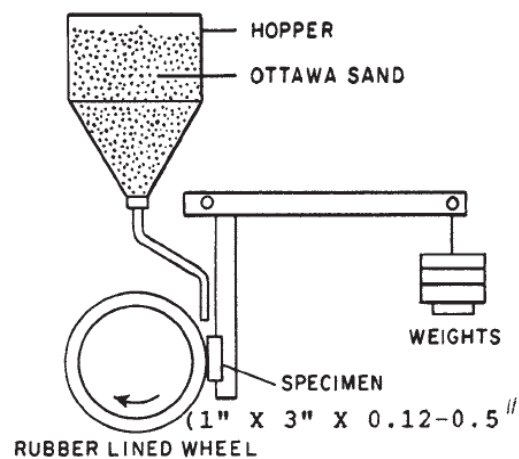
Figure 7: Schematic of assembly for the ASTM G65 test [45]

ASTM C633 standard test

ASTM C633 or the "Standard test method for adhesion or cohesion strength of thermal sprayed coatings" [43] is a test to determine the degree of adhesion or cohesion of a coating to the substrate. In this test a specially made cylindrical (1inch diameter) substrate was coated with the flame sprayed titania and an adhesive bonding agent is used to glue the surface of the coating to one side of an special rod which is clamped by a tensile machine. After curing, the tensile force is applied until the coating fails. The fractured surface and the tensile force will then be analysed to study the behaviour of the coating.
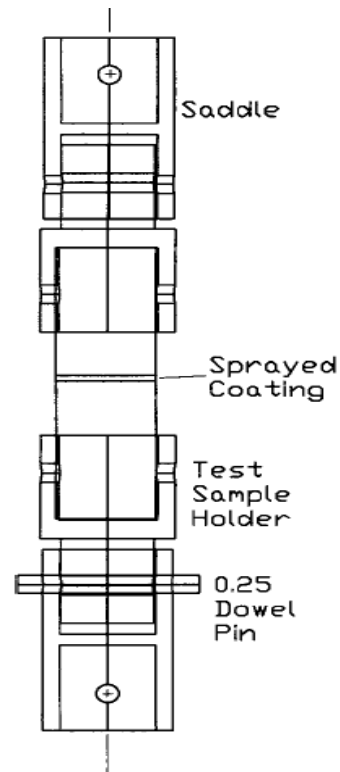
Figure 8: Schematic of the assembly for the ASTM C633 test [43]

Figure 8 shows a schematic of the tension testing machine clamp which is glued to the coating's surface. Exact dimensions and specifications of the test can be found in the ASTM C633-01 standard [43] document.

Confocal Microscopy

Confocal microscopy is a technique to study and analyze uneven surfaces. The technique takes advantage of a special microscope called

confocal microscope. This microscope is coupled with an analyzing software that can provide topographic images from the damaged or worn surfaces. In this study, a white light confocal microscope was used to provide a topographical view of the surface of the titania coatings.
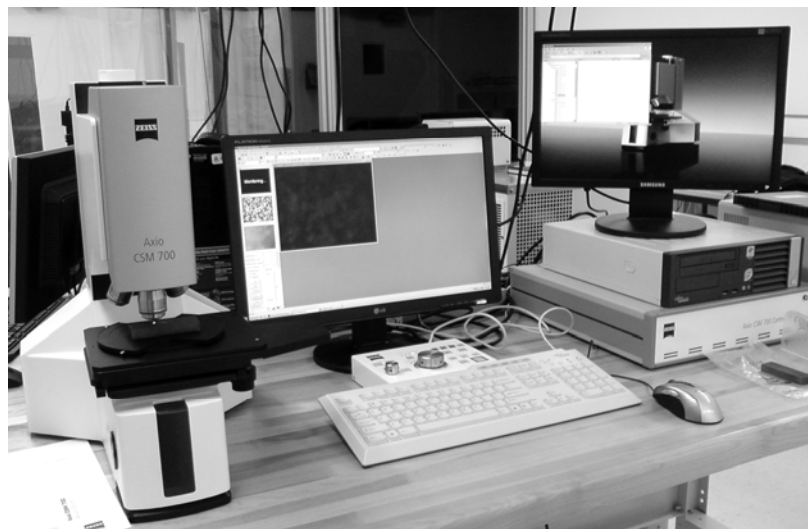
Figure 9: Axio CSM 700 Confocal microscope

The white light confocal microscope, which was used to analyze the samples, was an Axio CSM 700 (Carl Zeiss Micro Imaging GmbH, Gottingen, Germany). A schematic of the confocal microscope is shown in Fig. 10.
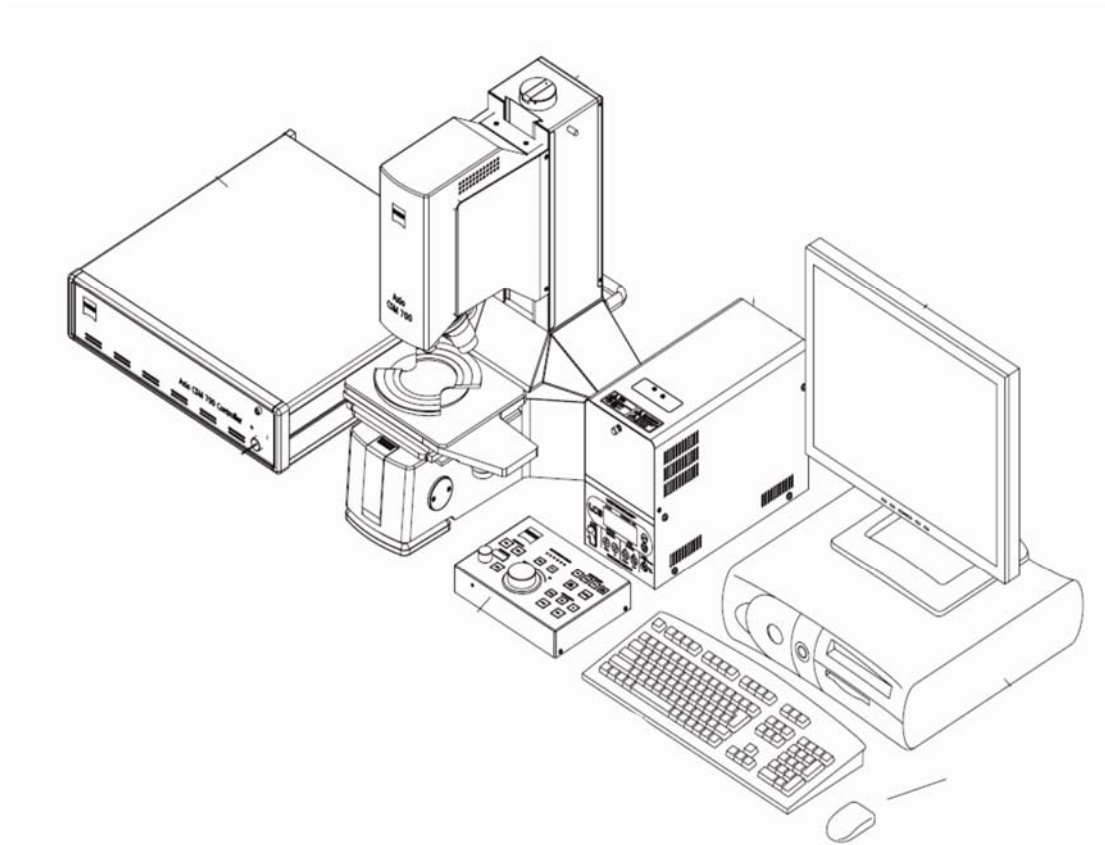
Figure 10: Schematic view of the confocal microscope [46]

Microscopy procedure

Prior to the microscopy, several things should be checked. The lamp should be stabilized and the working distance should be adjusted. The microscope can be controlled by the software afterwards. The software which is used to analyze the data (Axio CSM 700) is installed on the main computer. A console is used that is connected to the main microscope unit using the control box to control the software. Figure 11 shows the software at live view. Before using the microscope a timing

adjustment should be done using the calibration glasses. After this step the microscope is ready to use for analyzing the samples.
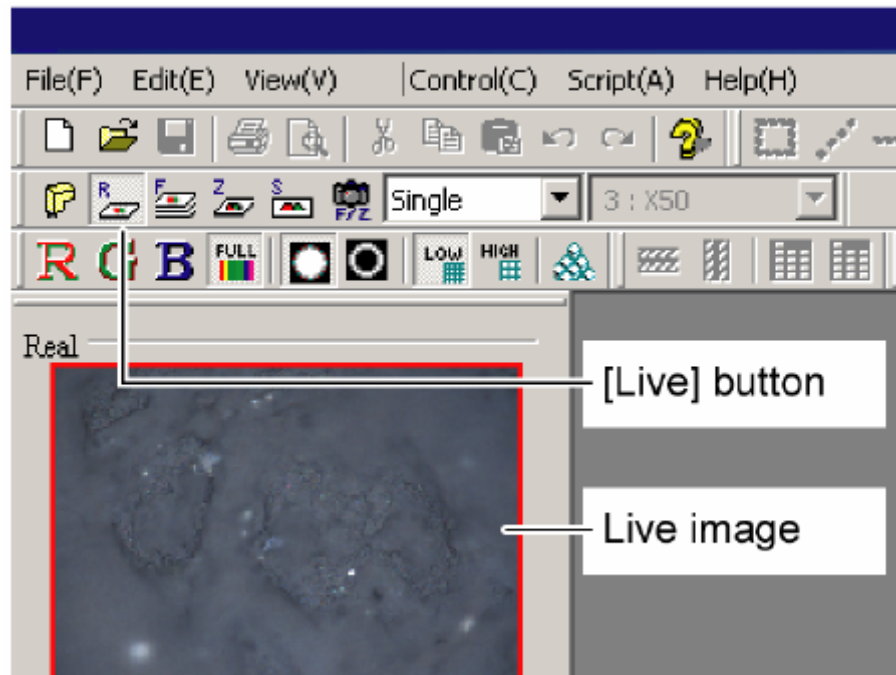
Figure 11: A view of the software which was used for analyzing the confocal microscope images [46]

When the sample is at the right place on the microscope's stage, the image can be focused by changing the stage height. After selecting a reference point and the upper and lower limits of vertical movement of the stage, the microscope is ready to scan the surface in different layers. The images presented in this study have all been taken at resolution of 0.5 micrometers and by using the 20 times magnification objective lens and with a total magnification of 339 times. The microscope will scan the surface layer by layer until it covers the whole

range and then it generates three sets of images including F-Image or All in focus image, which all the points of the image is focused in one picture, Z image which has the z axis information of the image, and an F-Z image which is a combination of the other two.

Using these images the software can calculate the surface roughness parameters and deliver them to the user. R_a, R_{sk} and R_{ku} are some of these parameters measured by the microscope to be used for analyzing the surface characteristics of the samples.

By using the 3D view option in the software, the computer will generate a three dimensional schematic view of the surface and delivers it as a graph. This can be used to compare different surfaces together and notice the differences between them. Pictures generated with 3D view will be discussed in and analyzed in following sections.

Confocal microscopy samples

Using the confocal microscopy, the worn and as-sprayed parts of both nanostructured and conventional titania coatings were studied. For each part 10 different points were scanned. A total of 4o points were

studied on the coatings. The results were then averaged and compared to each other. The samples were studied with confocal microscopy was subjected to the ASTM G65 test with 250 revolutions before the microscopy.

X-ray diffraction

As a powerful tool to investigate the phase composition of the materials X-ray diffraction (XRD) was used to study the present phases in the coatings. Coated samples were cut to the appropriate size of 1cm long by 1cm wide and the thickness of approximately 4mm. The coatings were then analyzed by a powder X-ray diffraction unit (RU-200B Line Focus X-Ray System, Rigaku Rotating Anode XRD System, Rigaku, Ontario, Canada) with a copper anode. 2θ angle was altered from 20° to 80° with a step size of 0.05° and a step time of 2.5 seconds. The results are discussed later in the present document.

H$_2$S test and Energy-dispersive X-ray spectroscopy

The coating made with 20psi of compressed air pressure was tested under gaseous corrosive environment to study its resistance against chemical attacks. Samples were placed in a quarts tube and inside a

resistant heated oven. Temperature was raised to 70° Celsius by a rate of 3° per minute. Once the proper temperature was reached, a mixture of hydrogen and 500ppm of hydrogen sulphide (H_2S) was pumped into the quarts tube. The coating was left in contact with the gas, moving with a flow rate of 60 millilitres per minute, continuously for 5 hours. Samples were then removed from the chamber and polished using standard metallographic procedure.

Energy-dispersive X-ray analysis was performed on the polished cross section of the coatings using a Zeiss microscopy unit (Zeiss EVO MA 15, Carl Zeiss SMT Inc. North America) equipped with EDX detectors. A total of 4 points on 2 samples were analysed and mapping and line scanning were performed on the samples. These results and other information gathered about flame sprayed titania coatings are further discussed in chapter 3 of this document.

C hapter 3

Results and discussion

Using the setup, which has been explained in the experimental procedure section, the coatings were deposited on the substrate. Both of the nanostructured and conventional titania was deposited using compressed air introduced into the torch. The pressure of compressed air varied from 5 to 50psi. These coatings were then studied using porosity measurement, hardness measurement and microscopy. Results were analyzed and large samples were made for ASTM G65 standard test. These new samples were made using a 20psi compressed air pressure, which performed the best in previous tests. After undergoing the standard procedure of ASTM tests the samples were studied by confocal microscope and the results were reported. In the present chapter these results are summarized in addition to the preliminary XRD and EDX analyses.

Hardness of the nanostructured and conventional coatings

An important factor in the quality of the coatings is the coating's hardness. It is obvious that a lower porosity level results in a higher hardness throughout the coating and a lower porosity is achieved through a high particle velocity. Comparing the coatings made by the High Velocity Oxy-Fuel (HVOF) spraying to the ones made by Flame Spay (FS) method, can give us an idea of the effect of particle velocity on the hardness and porosity of the coatings [2]. These facts suggest that for making a harder coating, it is necessary to accelerate the particles before hitting the substrate. The acceleration could be achieved by introducing compressed air into the flame of the flame spray torch. To study the effect of compressed air, coatings were made by introducing a range of compressed air pressures from 5 to 50 psi into the flame. Vickers micro-hardness test results has been collected and shown in Fig. 12. A minimum of 6 hardness tests were done for each hardness average value and the Standard Deviation (SD) of these results was calculated and shown as error bars. According to the standard, if a pore happens to be on one of the tips or the indent hit a very large pore, the sample should be re-indented. In other cases the pore does not cause the indentation to be rejected. The presence of

these pores in the microstructure of the coatings was the reason behind the large error bars shown in the hardness graphs.
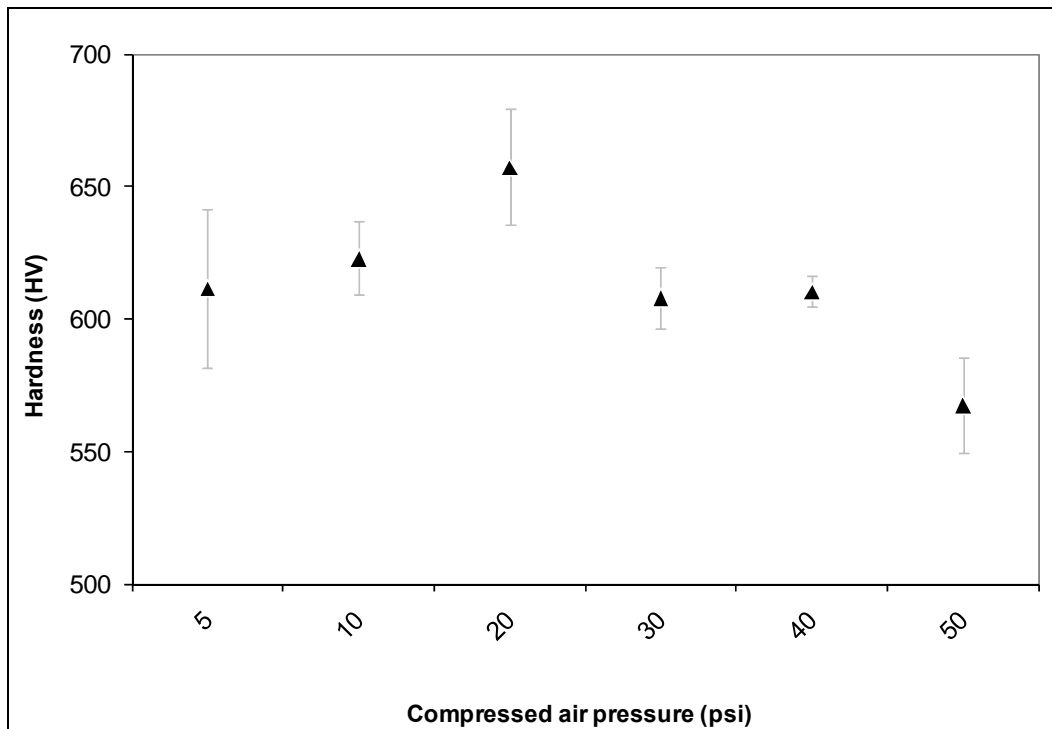
Figure 12: Vickers micro hardness vs. compressed air pressure for nanostructured coatings

Similar tests were done on the conventional titania coatings as well. The coatings were fabricated similarly and the microhardness test was performed on them. Figure 13 shows the results of these tests as well as the standard deviation in the form of error bars.
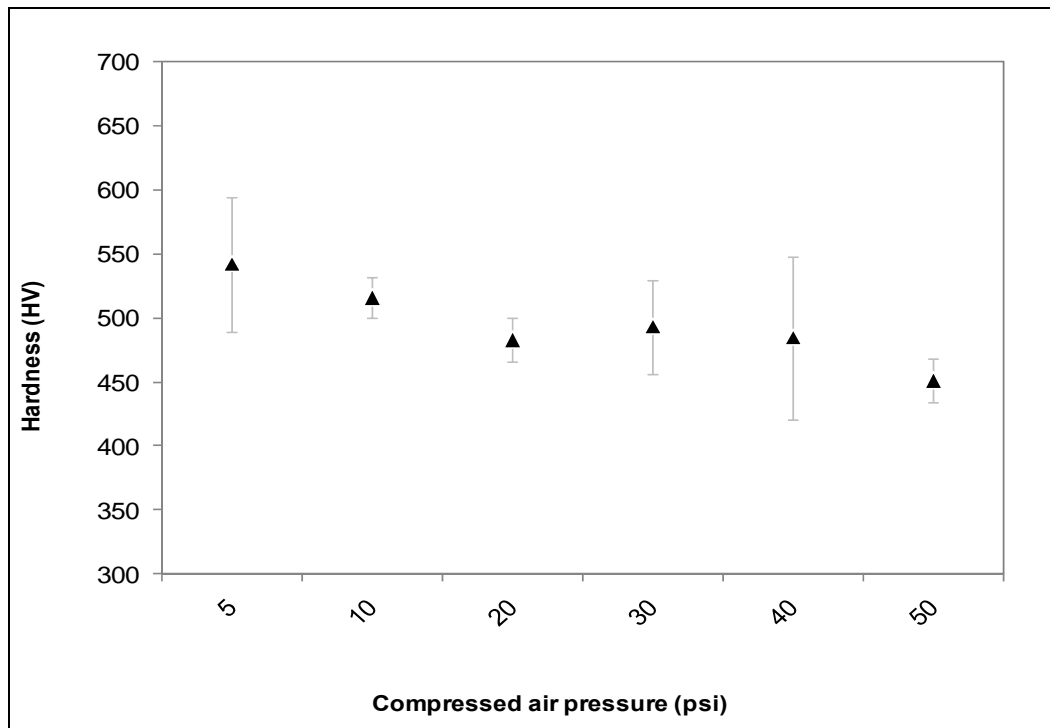
Figure 13: Vickers micro hardness vs. compressed air pressure for conventional coatings

It is obvious from Fig. 12 that nanostructured titania shows its best performance while sprayed with 20psi of compressed air. The hardness drops at higher compressed air pressures. On the other hand the conventional titania coating demonstrates a peak at the beginning of the chart and the average hardness value drops afterwards.

It is common to link the higher hardness values of a coating to their higher wear resistance. But common wisdom does not apply to the nanostructured coatings. Researchers observed different connections between hardness and wear performance of these sorts of coatings. As

an example nanostructured alumina-titania ceramic coating, with a lower hardness value compared to its conventional coating, was shown to perform much better under wear testing [21]. On the other hand it has also been observed that nanostructured alumina coatings have higher hardness and wear resistance both at once, when compared to their conventional counterpart [10].

In case of nanostructured titania the wear resistance is linked to various reasons which will be discussed later on. But as it is observed in Figs. 12 and 13, it can be mentioned that the nanostructured titania coatings made by flame spraying are showing higher values of hardness when compared to the conventional ones. Higher values of recorded hardness in nanostructured titania is not only affected by the intrinsic hardness of the ceramic material. This value, according to the nature of thermal spraying, also depends to the inter-lamellar adhesion and mechanical bonding of the splats. Lack of inter-lamellar adhesion plays an important role in measurement of the hardness values, by failing and opening the way under loading imposed by the indenter's tip. A coating with higher inter-lamellar adhesion like the nanostructured coatings with nanozones spread in the splat boundaries is then supposed to have higher hardness values when compared to the one with a weaker inter-splat adhesion [47]. These

hardness values are also affected by porosity levels of the coatings which will be measured in the following section.

Porosity measurements

Porosity of the coatings was measured by image processing techniques using the scanning electron microscope images that were taken from the cross section of the coatings (Fig. 15 and 17). Image-Pro Analyzer 6.3 (Media Cybernetics Inc. Bethesda, MD, USA) was used to measure the porosity from the SEM Images. The porosity can be altered by changing the velocity of the particles that impact and spread on the substrate [2]. This effect has been studied along with the hardness measurements by changing the pressure of the compressed air that was introduced into the flame spray torch. This pressure was changed to the values of 5, 10, 20, 30, 40 and 50psi and the porosity of the coatings were measured. The average porosity was calculated and the results are as presented in Fig. 14.
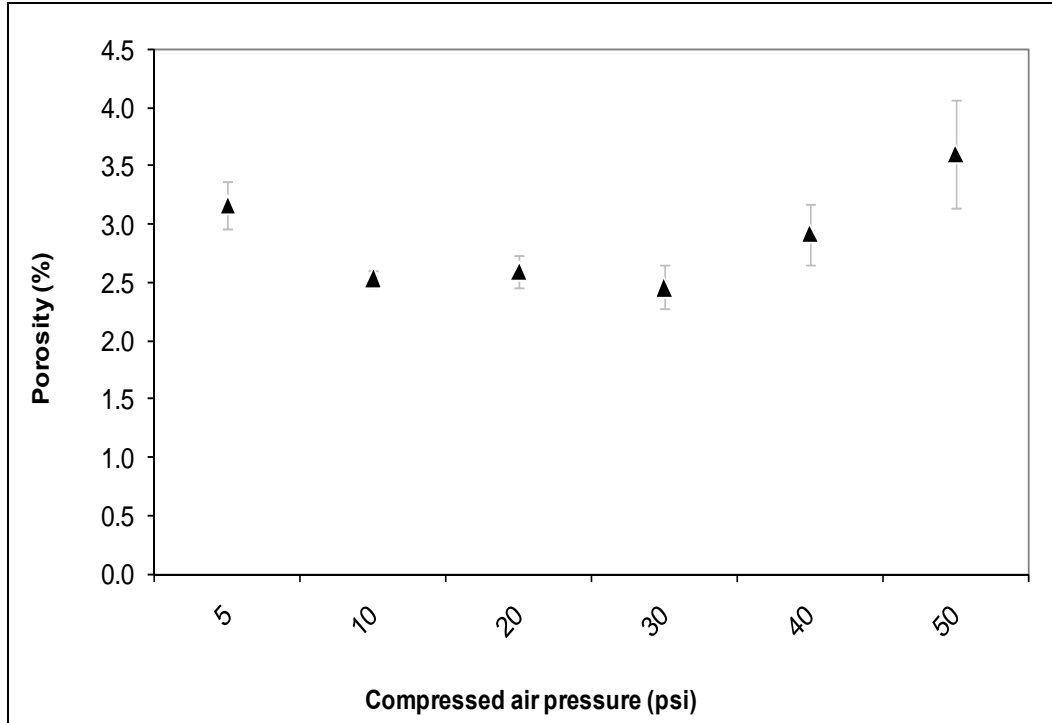
Figure 14: Porosity of the nanostructured titania coatings vs. compressed air pressure introduced into the torch

From the graph it is obvious that the porosity is at its lowest when the compressed air pressure level is almost at 20psi and the most porous coating happens when the pressure is 50psi. The porosity measurements showed a decreasing trend by introducing the compressed air into the torch. This trend did not continue by increasing the pressure of the compressed air, on the other hand the porosity level was seen to be rising after the pressure of the compressed air is increased to values more than 30psi.

5 psi

30 psi

10 psi

40 psi

20 psi

50 psi
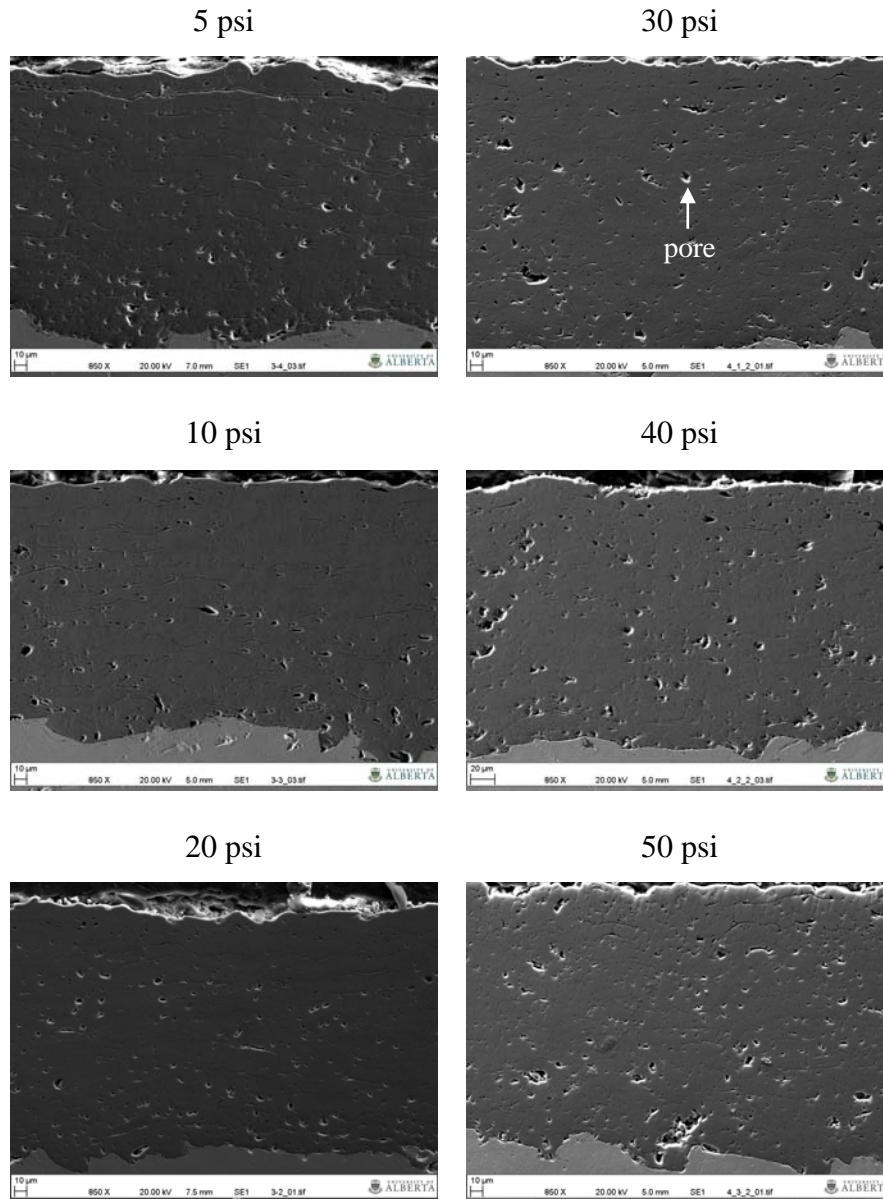
Figure 15: Images from the nanostructured samples for porosity measurements

Increase and decrease of the hardness values in Fig. 12 seem to be following the reverse trend of the porosity graph (Fig. 14). This fact can be the result of the large impact that the porosity can impose on the hardness, due to the microhardness measurement procedure. Porosity of conventional titania coating samples made by compressed air

pressure of 5, 10, 20, 30, 40, and 50psi were also measured by the same technique and the average porosity values are illustrated in Fig. 16.
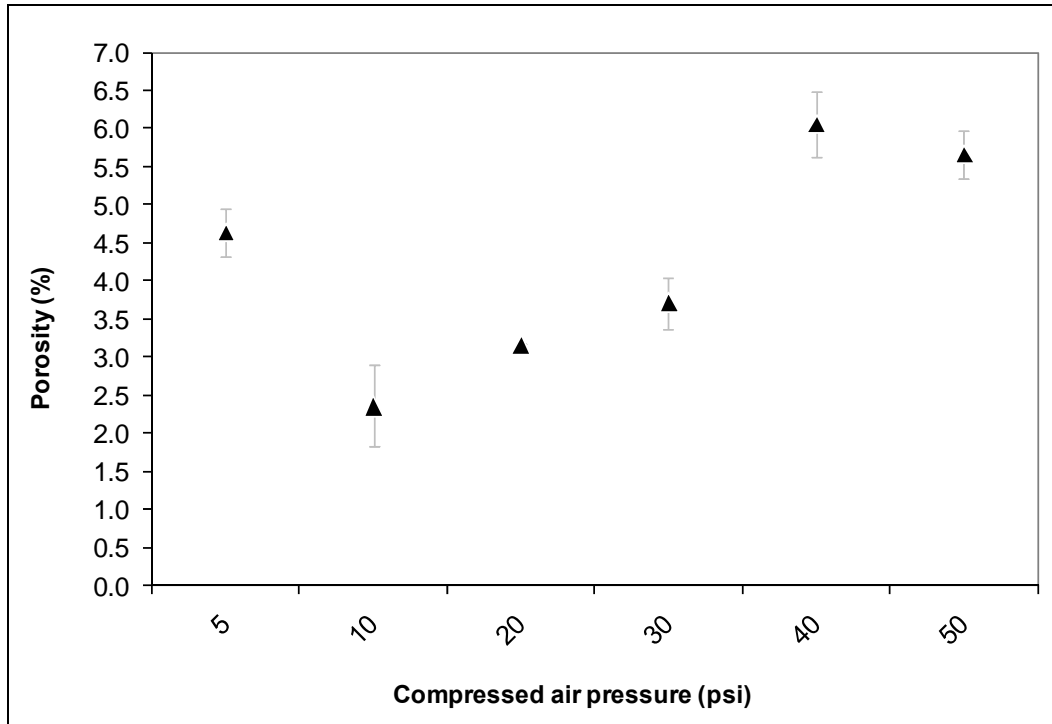
Figure 16: Porosity of the conventional coating vs. compressed air pressure introduced into the torch

The same sudden decreasing trend is observed here as well by increasing the compressed air pressure. The measurements again show an increasing trend in porosity level when the compressed air pressure in the torch is further increased. The only difference is that in conventional titania the minimum porosity happens at compressed air pressure of 10psi while this minimum happens in 20psi in nanostructured titania. SEM images which are representative of the

coatings for different amounts of compressed air are shown in Fig. 17. These images were used to measure the porosity of the conventional coatings.
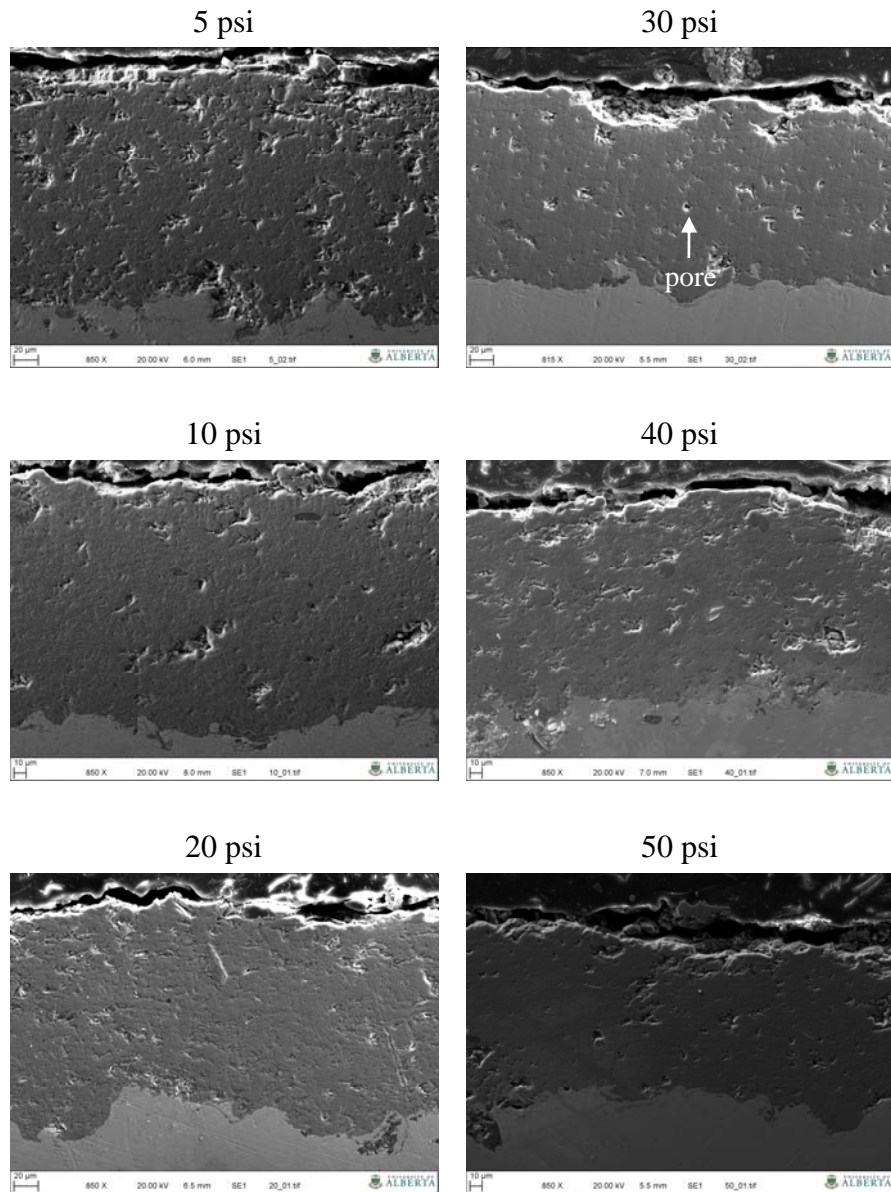
Figure 17: Images from the conventional titania coating samples made with different amounts of compressed air pressure and used for porosity measurements

Hypothesizing the effect of compressed air on the quality of the coating

It is generally accepted that a denser coating is made by higher velocity and higher temperature particles. The reason that HVOF coatings have lower porosity levels are the higher kinetic energy that the particles have while reaching the substrate. The kinetic energy increases the droplet deformation at impact and results in filling the pores in the produced coating [48]. In flame spray process the particle temperature is higher than HVOF and Air plasma spraying (APS) and the particle velocity is lower than both of these methods [2]. Adding compressed air to the flame spraying torch should have an increasing effect on the velocity of the particles but a decreasing effect on their temperatures. Therefore introducing the compressed air to the flame spray torch can have both increasing and decreasing effect on the porosity level and consequently the hardness of the coatings. In this study, the optimum amount of compressed air to deliver lowest porosity of the coatings was determined.

The trend which is observed at the porosity vs. compressed air pressure graph for nanostructured coating (Fig. 14) is showing a decrease at the beginning of the curve by increasing the compressed air

pressure. The decreased porosity can be explained by the higher kinetic energy of the coatings which contact the underlying splats. The faster the molten or semi molten powder particles hit the surface of the substrate the more penetration of the molten part into the pores of the splats is going to happen. Therefore, a denser coating is expected to be made [42]. The same trend was also been noticed in the conventional coating's (porosity vs. compressed air pressure) graph at Fig. 16, which can also be justified with the higher particle impact kinetic energy.

When the amount of compressed air is increased beyond a certain level, the trend is reversed and the porosity of the coating is seen to be increasing. In flame spray process the temperature that is reported by the literature as the particle temperature, is actually the temperature of the outer surface of the particles. In this process there are always some semi molten particles left in the flame which will be deposited on the substrate at impact. In case of nanostructured titania these semi molten particles carry the nanostructured regions from the powder feedstock to the coating. If the temperature of the torch decreases drastically, the percentage of these semi molten particles will increase in the flame and vice versa. Since the amount of fully molten titania droplets are supposed to be less in a flame with lower temperature, the droplets produced by this flame are less prone to infiltrate inside of the

underlying splat pores to make the coating denser. This is probably the reason behind what is happening inside the flame spraying torch, which results in coating to be more porous, when the compressed air pressure is increased beyond a certain level. The same argument can be used in case of conventional titania coatings as well. Another interesting point can be the fact that the splats made by higher velocity droplets, tend to fragment at impact. This might probably result in a coating with higher porosity levels and the decreasing trend in the graph can also be described with mentioned hypothesis.

Another possible explanation of the increasing porosity could be the air entrapment hypothesis. Looking at the SEM images (Figs. 15 and 17) it can be noticed that by increasing the pressure of the compressed air the pores are changing in shape from fine pores to less occurring larger pores. By addition of the compressed air to the torch, the probability of these pockets of air getting trapped between the depositing splats will increase. The larger pores detected by SEM imaging of the coatings are probably the same pockets of air entrapped in between the titania splats. This phenomenon joined by the temperature of the particles make it possible to explain the reason behind the difference of porosity level in coatings sprayed with different pressures of compressed air.

Abrasive wear testing (ASTM G65)

As mentioned in previous chapter, standard samples of the nanostructured and conventional titania coatings were made and the samples were exposed to the ASTM G65 standard test. The test consists of a wheel which grinds the coating's surface and a nozzle which feeds quartz grain sand between the coating and the wheel. At the first stage of the test the 3" by 1" by 0.5" specimens were tested under 6000 revolutions of the test wheel. The test was too rigorous for the titania samples and the whole coating and a part of the substrate was worn away. Figure 18 shows the scars left on the samples after 6000 revolutions of the wheel.
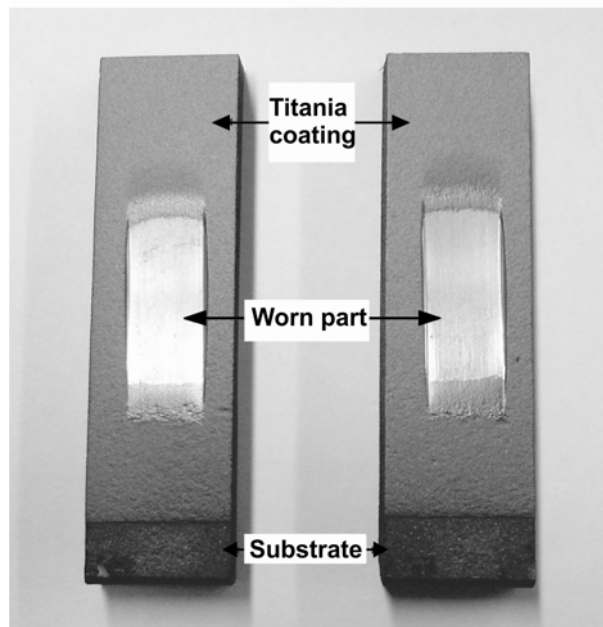
Figure 18: Wear scars from ASTM G65 test after 6000 revolutions of the wheel on nanostructured titania coating.

The mass losses for these nanostructured specimens were calculated by weighing them before and after the test and these data were summarized in the following table.

Table 2: Mass loss for nanostructured titania under ASTM G65 with 6000 revolutions of the wheel

Sample	Initial mass (g)	Final mass (g)	Mass loss (g)
1	205.81	204.389	1.422
2	206.205	204.758	1.448

In this set of results the wheel pierced through the coating and hit the substrate underneath the coating. For this reason the results are not valid for analyzing the performance of the titania coating. To determine the performance limit of the coating in less extreme wear conditions, samples were exposed to the ASTM G65 test with a decreased total wheel rotation of 250 revolutions. Better performance of ceramic coatings in lower revolutions of the test wheel was also reported by Bolelli *et al.* [38]. After this modification it was observed that the nanostructured coating was capable of withstanding the rigorous test condition, but the conventional coating was completely eroded away and the wheel reached the substrate underneath the coating. Figure 19 shows the specimens after being exposed to the ASTM G65 test.
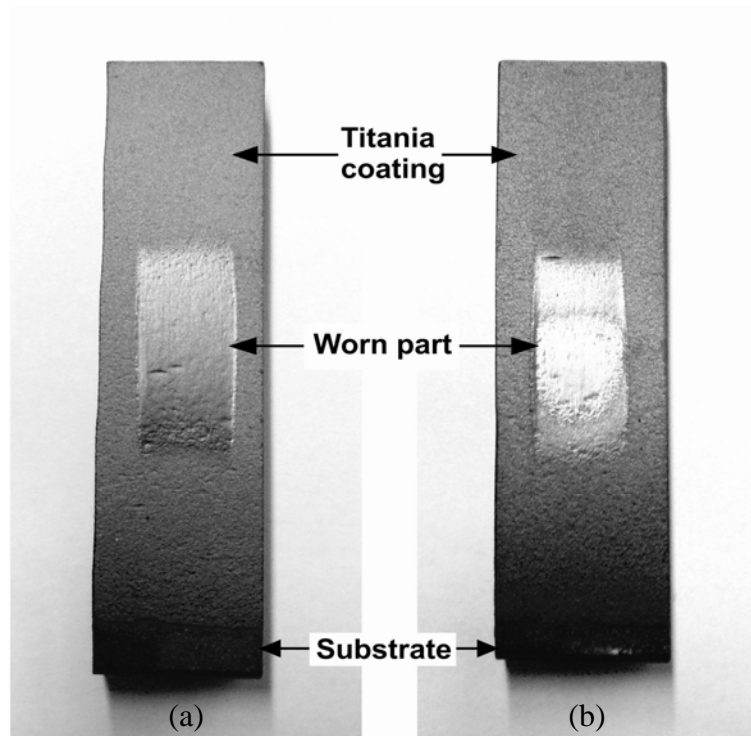
Figure 19: (a) Left: Nanostructured and (b) Right: conventional titania samples after being exposed to the ASTM G65 test with 250 revolutions of the wheel

The mass loss during this test was calculated and summarized in the following table.

Table 3: Mass loss for nanostructured and conventional titania coatings under ASTM G65 test with 250 revolutions of the wheel

Specimen	Mass loss (g)
Nanostructured titania	0.047
Conventional titania	0.220

The figure shows that while the conventional titania coating was nearly completely removed, exposing the bare steel substrate, a portion of the nanostructured titania coating remained on the surface of the steel. To have a better idea we can calculate the mass loss per each revolution of the test wheel. The mass loss for the nanostructured titania was measured to be 1.8×10^{-4} g per revolution of the abrasive wheel (for 250 revolutions), with the total volume loss estimated to be approximately 11.4 mm^3 (The density of the titania which is 4.23 g/cm^3 and the appropriate porosity level was used to calculate these values. For example the volume loss for the nanostructured titania with 2.59% porosity was calculated as 0.047/((1-0.0259)*4.23) which is equal to 0.0114 cm^3). In the case of the conventional TiO_2 coating, the mass loss was significantly higher at 8.8×10^{-4} g per revolution and the total volume loss was approximately 53.7 mm^3. These results indicate that under the rigorous abrasion to which the coatings were exposed in the ASTM G65 testing, the mass and volume losses of the conventional TiO_2 coating were nearly 5 times larger than that of the nanostructured TiO_2 coating. It should also be mentioned that in case of the conventional coating, the reported mass loss may be impacted by the mass of the steel grinded away from the substrate and the difference might be smaller than what was calculated here.

Wear behavior of titania coatings

By running the ASTM G65 test on the samples it was observed that the nanostructured samples were capable of withstanding the 250 revolutions of the test wheel (Fig. 19(a)). On the other hand, the conventional coating failed to do so and the wheel grinded the whole coating away, reaching the substrate beneath (Fig. 19(b)). The reason for such a behavior can be found in the mechanism of material removal from the coatings.

During the wear of a ceramic material such as titania, both plastic deformation and brittle fracture of the ceramic might occur. This behavior depends on the nature of the ceramic material which is being tested. There is an important parameter in ceramics called the critical depth of cut. When the critical depth of cut is reached, the behavior of the ceramic will change from plastic deformation to brittle fracture and chipping [2]. Figure 20 shows a wear scar on the nanostructured (a) and conventional (b) titania coating. The scar on the nanostructured coating looks smeared and plastic deformation and plowing seems to be major deformation and material removal mechanism. On the other hand the conventional titania coating is full of debris and the scar looks like it is broken at different places. So, fragmentation in the form

of brittle fracture is more possibly the material removal mechanism [49].

Malkin *et al.* [50] derived an equation for critical depth of cut in a ceramic material as:

$$d_c = \beta \frac{(\frac{E}{H})}{(\frac{H}{K_c})^2}$$
Eqn. 1

Where d_c is the critical depth of cut, E is the elastic modulus, H is the hardness, K_c is fracture toughness and β is a constant. From this equation it is obvious that the critical depth of cut (d_c) is directly proportional to square of toughness to hardness ratio for each ceramic. Now going back to the nanostructured and conventional titania coatings we can understand from Fig. 20 that the nanostructured coating has a smooth surface and plastic deformation and plowing is the major material removal mechanism while the major mechanism in conventional titania is chipping and brittle fracture. In other words it can be said that the nanostructured titania has a larger depth of cut when compared to the conventional counterpart [49].

Taking into consideration both the larger depth of cut of the nanostructured titania and the proportionality from the Eqn. 1 lead us to an interesting fact about these coatings. According to the Eqn. 1 nanostructured titania should have a higher toughness to hardness ratio than the conventional coating. Since even the hardness of the nanostructured titania is larger in value than the conventional counterpart (Figs. 12 and 13), one can come to a conclusion that the toughness of the nanostructured titania coatings are probably much higher than that of the conventional titania coating. This toughness of nanostructured titania was measured through indentation (crack propagation resistance) and will be discussed later in this chapter.

(a)

(b)
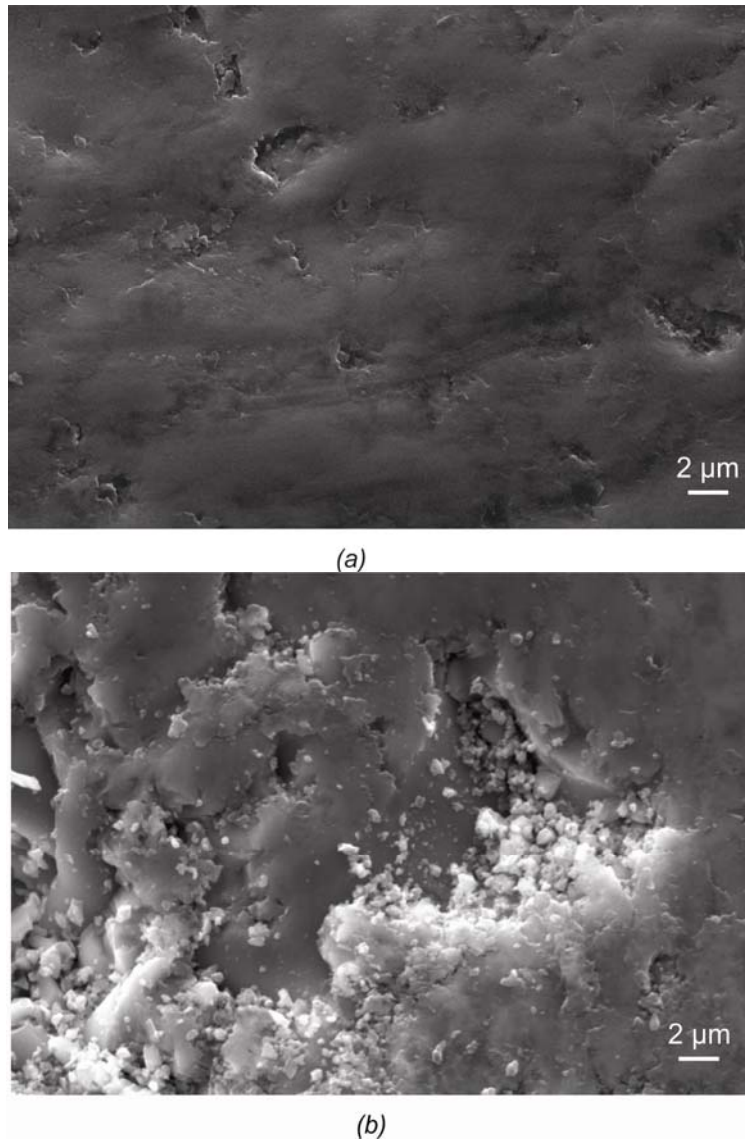
Figure 20: SEM images of the wear scars (a) nanostructured TiO_2 wear scar looks smooth and plastically deformed (b) conventional TiO_2 scar looks rough and the brittle fracture remnants are visible.

Fine porosity and stratification

By looking at the SEM images of nanostructured titania (Fig. 15) it is obvious that increasing the compressed air affects the coating in case

of both porosity and stratification. The porosity in thermal sprayed coatings is divided into two categories of coarse and fine porosity. The coarse porosity happens because of 1. failure in completely filling the gaps while making the coating from splats (splat stacking), 2. unmolten particles or 3. gas entrapment [38]. This sort of porosity has been discussed before. Second sort of porosity or the same horizontal lines in the cross section of the coatings are the boundaries between different layers of splats, which form the coating. These lines are called the fine pores, which are always present in the thermal spray coatings because of the nature the process [26].

According to the SEM images, these so called fine pores seem to be thicker and longer in coatings made by lower compressed air pressures and they get thinner and almost fade away by increasing this pressure in the torch. The reason behind this kind of behavior can be the higher impact velocity of the droplets which force the molten parts of the splats to infiltrate into the inter-lamellar gaps and fill them. This impact velocity increases as the compressed air pressure increases.

Another thing that can affect the splat stacking in the thermal spray coatings is the low roughness of the well spread splats that decreases the mechanical adhesion of new-coming droplets. The presence of semi

molten nano zones in between the splats (Fig. 27) can probably lead to increased roughness in the as sprayed surface of the nanostructured titania while comparing it to the conventional counterpart [38]. The increased surface roughness will help to strengthen the mechanical interlocking between the underlying splat and the molten droplet which sits on it, forming the new layer of the coating. Better interlocking between the splats can also impede inter-splat crack growth and consequently affect the toughness of the coating in a positive way, as well as decreasing the stratification and the level of fine porosity in the nanostructured coating.

It is worth mentioning that the lower porosity in the thermal spray coatings is desirable in the wear resistance application. However, there are several applications of thermal sprayed coatings which porosity plays an important role in them. In biomedical applications and especially in orthopedic applications, it has been shown by researchers that a more porous ceramic coating with interconnected pores is useful for bone attachments and compatibility with the human body [51,52]. On the other hand, a pore-free coating is desirable to reduce the release of ions by metallic implants inside of the human body [42,53]. Therefore the application of thermally sprayed coatings is important in the approach toward dealing with the porosity in this sort of coating.

Confocal Microscopy

Confocal microscopy is an optical imaging technique for studying surfaces which are not smooth enough for regular microscopy [54]. This technique was used to study the surface topography of the conventional and nanostructured titania coatings deposited using the flame spray process. The coatings were subjected to severe wear conditions in ASTM G65 [45] tests with 250 revolutions of the wheel. The worn surfaces of the coatings were imaged as well as their as-sprayed surface and the data was extracted from the F-Z Images using the Axio CSM 700 software.

Surface topography

A 3D view of the surface was generated by the software for each of the 10 points that was selected and imaged for the scar and as-sprayed sections on the nanostructured and conventional coatings. Comparison between the worn section and the as-sprayed section of each coating shows a great difference in the surface topography. But the slight difference which is noticed between the worn part of nanostructured

and conventional titania is of great importance. These differences and the reasons behind it are going to be discussed.
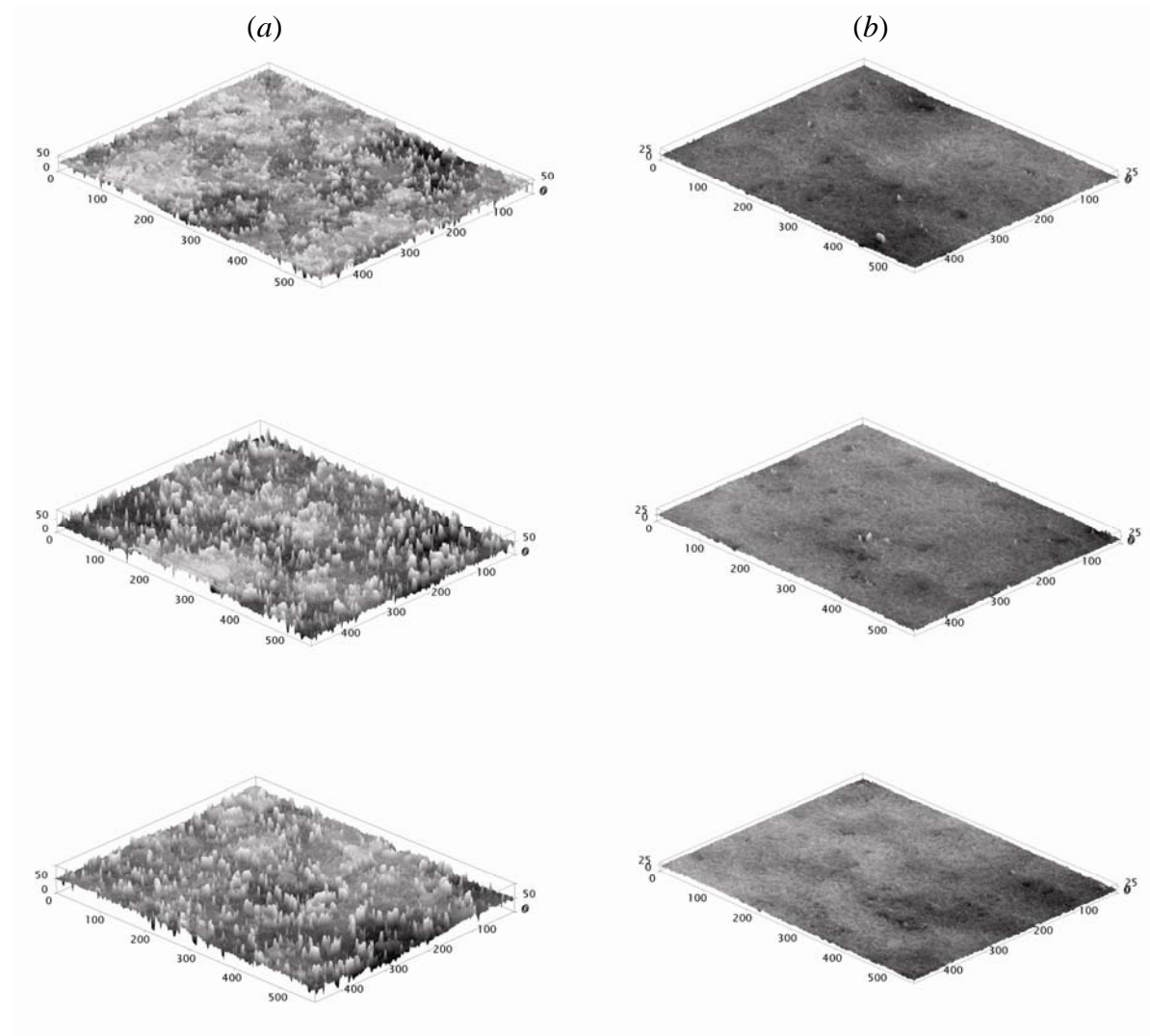
Figure 21: 3D surface images of the (*a*) as-sprayed and (*b*) worn sections of the nanostructured titania coatings (Scales are in micrometers).

(*a*) (*b*)
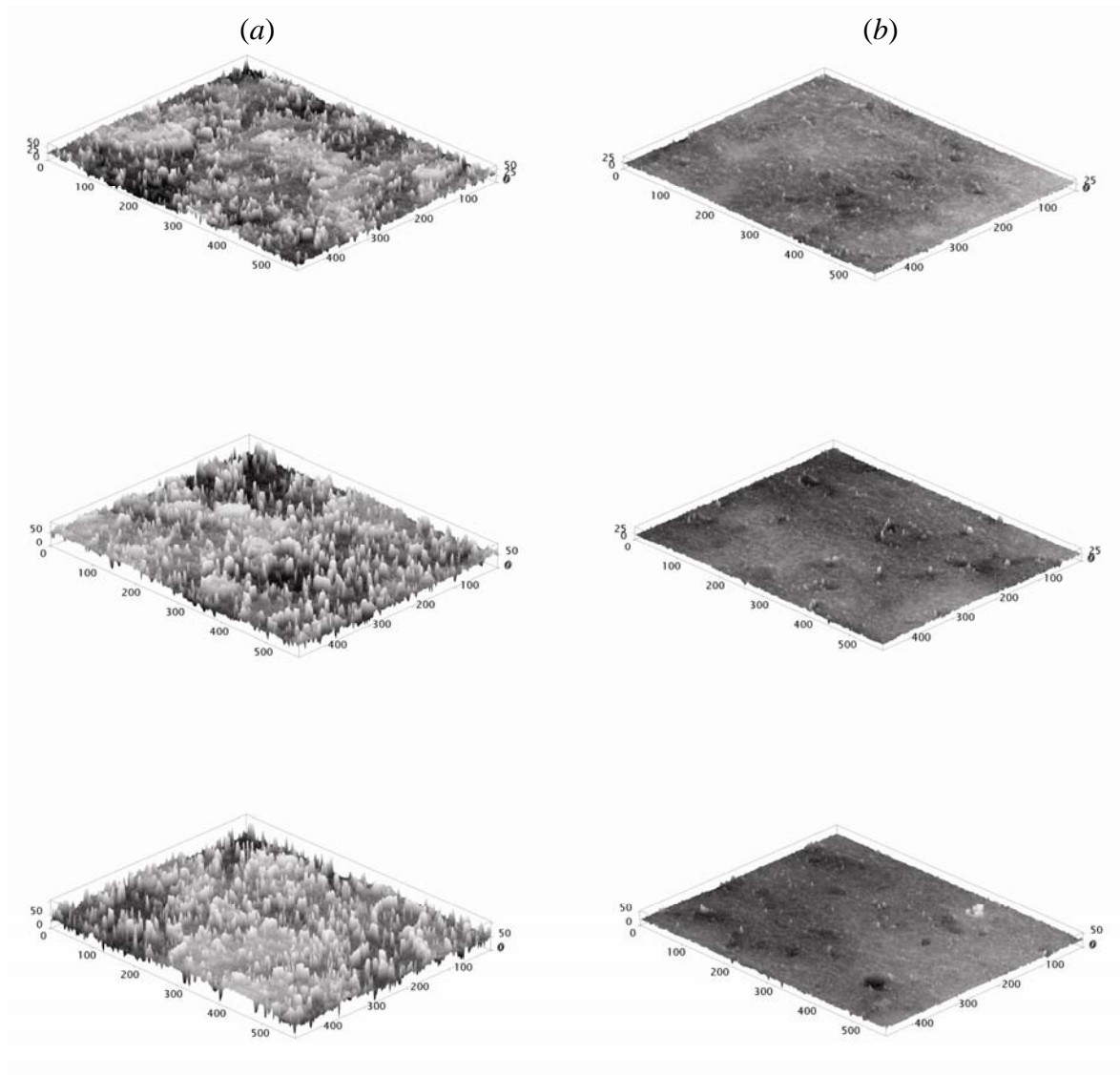
Figure 22: 3D surface images of the (*a*) as-sprayed and (*b*) worn sections of the conventional titania coatings (Scales are in micrometers).

This analysis was done for ten points on the scar and ten other points on the as sprayed part of the nanostructured titania coatings. The same was done with the conventional titania coatings. Figs. 21 and 22 are representative images of the topography of the surface. The comparison between these surfaces can give us an idea of how the

coating behaves when put under the ASTM G65 standard test. In both Figs. 21(b) and 22(b) it is obvious that the coating has been worn away after being exposed to the G65 test. Focusing more on these two sets of images reveals a smoother surface in case of the nanostructured coating. This statement is further proved by the noticeable change in colors and higher number of pits obvious on the surface of the conventional coating (Fig. 22(b)).

Surface roughness parameters

To understand and quantify the differences between these two surfaces, the surface profile has been analyzed by the Axio CFM 700 software and the different surface parameters have been calculated automatically. These parameters can give us a quantified understanding of the surface. Results were summarized and the surface parameters describing the characteristics and topography of the surface such as average surface roughness (R_a), surface skewness (R_{sk}) and surface kurtosis (R_{ku}) were presented in the tables 4, 5, 6 and 7.

Table 4: Surface parameters for the worn section of the nanostructured titania coating samples

Nanostructured TiO$_2$	R_a	R_{sk}	R_{ku}
Scar1	2.047	-0.35	3.106
Scar2	2.088	0.09	4.097
Scar3	2.63	0.339	2.717
Scar4	2.371	-0.066	3.284
Scar5	1.97	-0.048	3.417
Scar6	1.763	-0.383	3.203
Scar7	2.403	-0.188	2.543
Scar8	3.625	0.249	2.401
Scar9	1.874	0.352	3.76
Scar10	2.524	0.328	2.741
Average	2.330	0.032	3.127
SD	0.538	0.282	0.542

Table 5: Surface parameters for the worn section of the conventional titania coating samples

Conventional TiO$_2$	R_a	R_{sk}	R_{ku}
Scar1	2.662	0.098	2.642
Scar2	2.394	0.388	3.669
Scar3	2.866	0.187	5.135
Scar4	2.321	0.178	4.253
Scar5	3.128	-0.08	3.454
Scar6	3.338	0.051	2.924
Scar7	3.113	0.353	3.432
Scar8	5.588	0.005	3.551
Scar9	7.19	-0.171	2.523
Scar10	2.633	0.126	3.521
Average	3.523	0.114	3.510
SD	1.590	0.175	0.767

Table 6: Surface parameters for the as-sprayed nanostructured titania coating samples

Nanostructured TiO$_2$	R_a	R_{sk}	R_{ku}
As sprayed1	6.311	-0.032	2.79
As sprayed2	9.763	0.465	3.636
As sprayed3	9.335	0.718	4.091
As sprayed4	9.213	0.634	3.753
As sprayed5	8.605	1.001	4.774
As sprayed6	9.383	0.797	4.022
As sprayed7	8.717	0.22	4.549
As sprayed8	9.998	0.992	4.664
As sprayed9	9.466	1.123	4.756
As sprayed10	7.931	0.561	3.942
Average	8.872	0.648	4.098
SD	1.082	0.362	0.622

Table 7: Surface parameters for the as-sprayed conventional titania coating samples

Conventional TiO$_2$	R_a	R_{sk}	R_{ku}
As sprayed1	7.238	0.407	3.183
As sprayed2	11.232	0.658	3.931
As sprayed3	11.88	0.243	3.523
As sprayed4	11.76	0.459	3.128
As sprayed5	12.167	0.076	3.842
As sprayed6	11.647	0.71	4.391
As sprayed7	12.341	0.497	3.502
As sprayed8	16.795	-0.148	2.841
As sprayed9	10.313	0.544	4.57
As sprayed10	9.701	0.672	3.913
Average	11.507	0.412	3.682
SD	2.411	0.279	0.553

By taking a look at these data it is possible to estimate how the surface looks after the test. For example, in case of R_a the value is much lower in worn part when compared to the as sprayed part (see tables 4 and 5). A slight decrease in the average roughness value has also been observed when comparing the conventional coating to the nanostructured one. This means that the nanostructured coating looks smoother according to the R_a measurements.

The values presented for R_{sk}, which measures the asymmetry of the surface profile, can provide useful information on the differences between the nanostructured and the conventional titania coating surfaces. The closer this value is to zero, the smoother is the surface. The values measured also show that the worn nanostructured titania coating surface is smoother than the conventional one with a value of 0.032 for the former and 0.114 for the latter.

A similar result was seen for the surface kurtosis (R_{ku}) which is the measure of the pointedness of the surface. For a perfectly random surface, this value should approach 3. A spiky surface tends to have a value close to 8 and a bumpy surface tends to have a value close to 0. The average value for nanostructured titania coating is 3.127 and the average for conventional one is 3.510, which represents a more pointed surface for the latter.
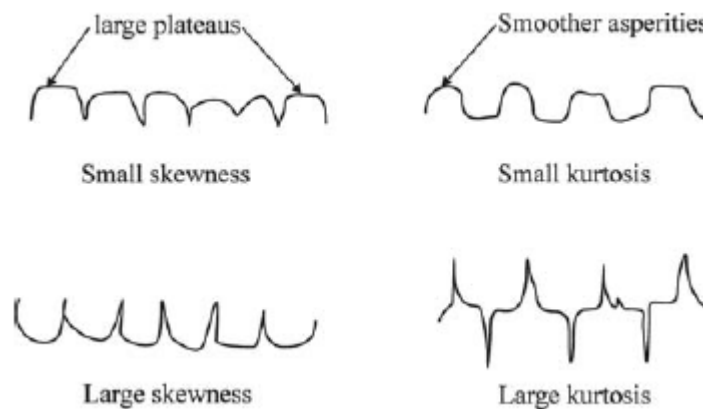
Figure 23: Schematic view of surfaces with different skewness and kurtosis values [55]

Using confocal microscopy, images were taken from the scar and the as-sprayed (unworn) section of the samples (Fig. 24). Unlike the optical microscope images, these images were focused on every point of the surface, which provides qualitative information on the smoothness of the surface. By looking at the images shown in Fig. 24, it is obvious that the scar left on the nanostructured coating appears to be smoother and that the titania coating is probably being smeared and smoothed by the wheel. On the other hand, the conventional coating shows signs of breakage and chipping, which appears as white dots in the image.

Scar		As-sprayed	
Nano	Conventional	Nano	Conventional
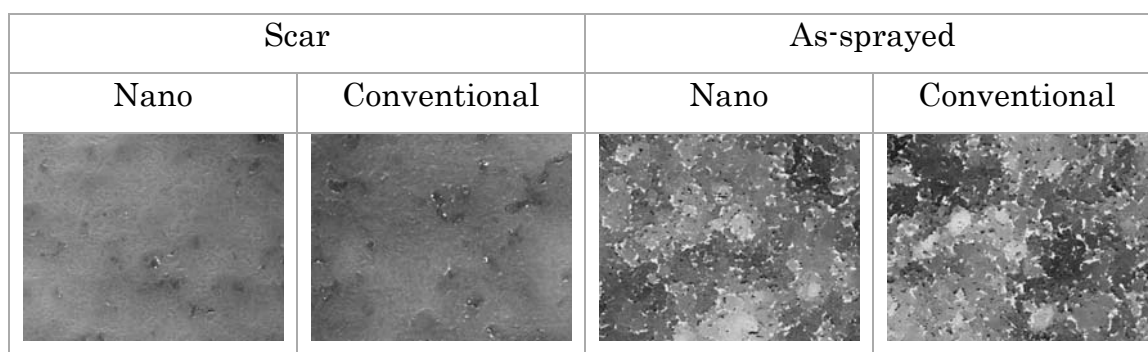
Figure 24: All in focus images from the worn and as-sprayed part of the nanostructured and conventional titania coatings

Superior performance of nanostructured coating

The nanostructured titania coating has shown a smoother surface than the conventional titania coating. This was concluded by comparing the

values for R_a, R_{sk} and R_{ku}. The results support the depth of cut theory explained before by showing a spikier surface for conventional titania coatings. A spiky surface with high surface kurtosis is a representation of the surface that is produced by brittle fracture in the ceramic. On the other hand a smooth surface like the ones in nanostructured coating with a kurtosis closer to three is indicative of plastic deformation in the coating. As it is obvious from the confocal microscopy results the nanostructured coating's scar shows a value of R_a and R_{sk} closer to zero and a value of R_{ku} which is closer to three than the conventional coating's scar. This supports the three different hypotheses that justify the plastic deformation of the nanostructured thermal spray coatings. The three hypotheses which are behind this behavior are as follows. First the crack arresting effect caused by the presence of dense semi molten ultrafine pockets embedded throughout the coating microstructure, second the better heat absorbing capacity of nanostructured particles which result in the higher temperature and lower viscosity of the molten part and produces better splat to splat adhesion and third the possibility of crack arresting by the presence of fine pored agglomerates embedded in the coating microstructure which hinder the crack propagation.

Another hypothesis points out the effect that splat surfaces have on the adhesion of subsequent molten powder droplets that impact the surface. The rougher the surface, the better is the mechanical bond between the solidified splat and the new one sitting on top of it. By looking at the average surface parameters for the as sprayed surfaces of the nanostructured and conventional titania, it is interesting that the nanostructured titania shows a higher amount of roughness than the conventional one (Higher R_{sk} and R_{ku} larger than three); this means that unlike the smoother surface of the nanostructured scar, this coating has a more uneven as sprayed surface than the conventional coating which results in better splat to splat adhesion.

Nano zones

Non-molten nanozones which are deposited in the coating can affect the quality of the nanostructured coatings in different ways. These zones can toughen the coatings as well as making them friable and abradable. Nano zones can be either dense or porous. Dense nanozones occur when the molten part of the semi-molten powder particles infiltrate into the non-molten part and fill its small capillaries during the spraying process. These dense nano zones can sit in between two

splats and arrest the cracks which are progressing through the inter-splat weak bond. The mentioned kinds of nano zones are helpful in the structure of the coating and they tend to increase the toughness. On the other hand porous nanozones can worsen the mechanical properties of the coatings [10].

Unlike other thermally sprayed ceramics nano zones in the nanostructured titania coatings are much harder to notice. To investigate the nanostructured structure of flame sprayed coating both scanning electron microscopy and X-ray Diffraction technique were used. Since the major phase in the feedstock powder is anatase and this anatase turns into rutile when melted and re-solidified (around 600 to 700 ºC) then it should be possible to get the percentage of each of these phases using XRD peak intensities and the equations developed by Berger-Keller *et al.* [39].

XRD

To investigate the phases present in the nanostructured coatings, samples were analyzed using the X-Ray Diffraction technique. Unlike what has been shown by the scanning electron microscopy, XRD pattern could not detect any anatase in the structure of the

nanostructured coating. The same thing has also been witnessed by the other researchers who studied the flame sprayed nanostructured titania [56]. The XRD results show rutile as the prominent phase in the coating's structure (Fig. 25). Rutile is produced after melting and resolidification of anatase, the prominent phase in the spray-dried nanostructured powder, used to deposit the coating. It is also possible that the anatase peaks and the amorphous titania, which can be present in the coating's microstructure, and is probably the result of rapid resolidification of the same anatase from the powder feedstock, are covered by the humps formed from peak overlaps. An XRD pattern for the nanostructured anatase powder has also been shown in Fig. 26, which shows the anatase peaks.
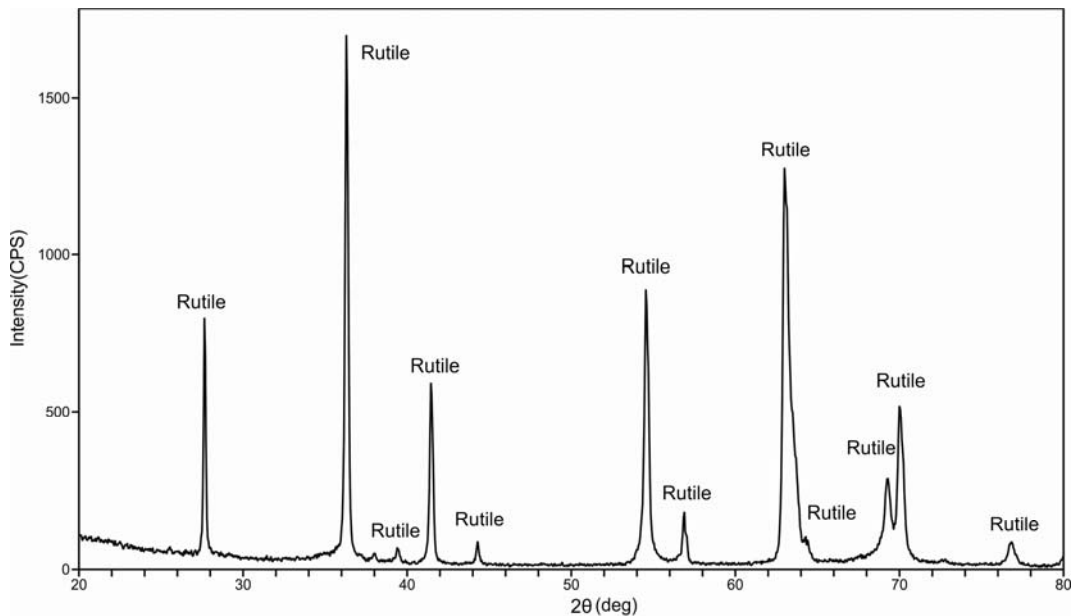
Figure 25: XRD pattern of the nanostructured titania coating made using flame spraying
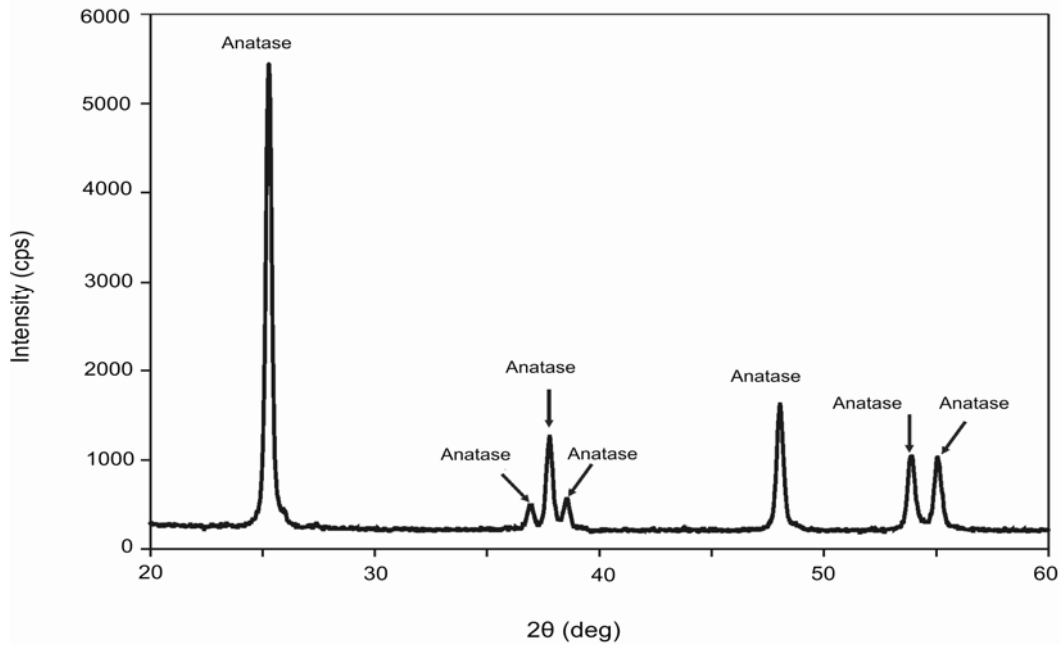
Figure 26: XRD pattern of the nanostructured titania powder [57]

Despite XRD results, the SEM micrographs of the coatings reveal the presence of the semi molten particles throughout the coating. Figure 27 shows the image taken from the as-sprayed surface and the polished cross section of the nanostructured coating. Presences of these semi molten particles are obvious in the structure of the coating in both of the images.

The high temperature of the flame spray torch is possibly the reason for researchers not being able to detect the anatase phase in XRD patterns (temperature range on the surface of the nanostructured titania powder particles can be as high as 2850 ºC in flame spraying). In case of detection of the anatase peaks in the pattern it is possible to calculate the volume percentage in the coating. The equation derived by Berger-Keller *et al.* [39] which is capable of measuring the volume concentration of anatase uses the peak intensities for both anatase and rutile to calculate the percentage. In this equation the volume percentage of anatase is derived to be equal to:

$$C_A = \frac{8I_A}{13I_R + 8I_A}$$ Eqn. 2

Where C_A is the concentration of anatase, I_A is the intensity of the [1 0 1] reflection of the anatase phase and I_R is the intensity of the [1 1 0] reflection of the rutile phase [58].
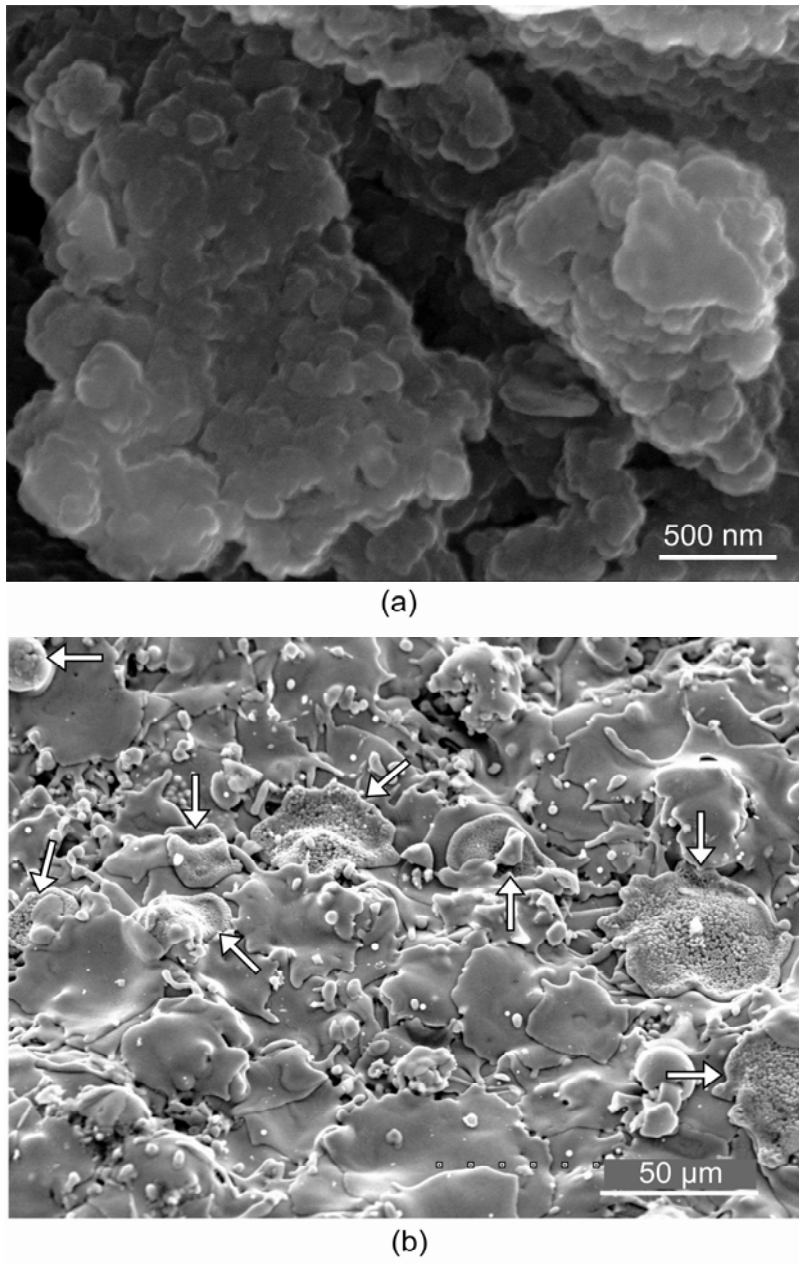
Figure 27: SEM images of the nanostructured regions in the TiO$_2$ coating (a) across the cross section of the coating and (b) on the as-sprayed surface (arrows show the semi-molten splats)

Crack propagation resistance

Crack propagation resistance is an important factor in degradation of the ceramic coatings and it is considered as a good measure for toughness of the coatings. To measure crack propagation resistance the equation proposed by Anstis *et al.* [59] was used. The polished cross sections of the coatings were indented with Vickers indentation instrument and the diamond formed with 1Kg of force in 15 seconds was imaged using the confocal microscope. The crack length initiating from the edges of the diamond was measured by image processing techniques and the crack propagation (K_c) was calculated as:

$$K_c = \frac{P}{c^{3/2}}$$

Eqn. 3

Where P is the load applied in newtons and c is half of the crack length from tip to tip in meters (Fig. 28).
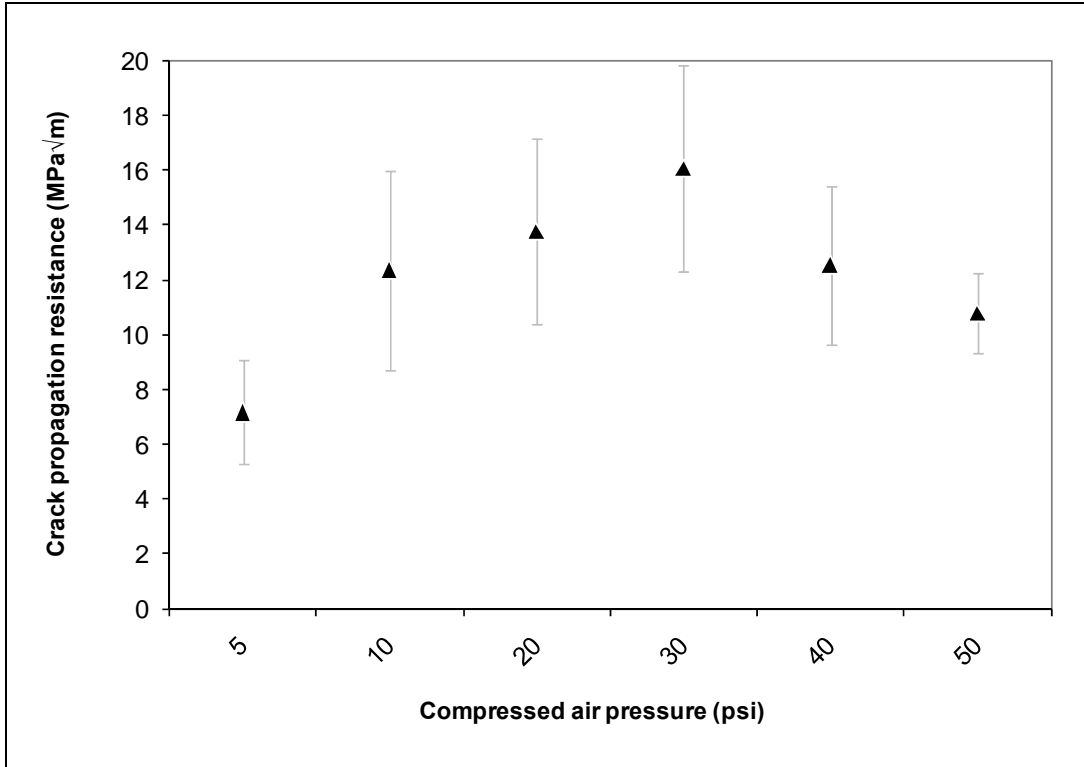
Figure 28: Crack propagation resistance of nanostructured titania coatings

The results indicate a maximum resistance at 30psi of compressed air introduced into the torch and the resistance is decreased by adding to the air pressure. The changes in the crack propagation resistance seem to be following the same trend as the hardness graph for the nanostructured titania in Fig. 12. The trend is also noticed to be present in inversed form in the porosity measurement graph of Fig. 14. These similarities are suggestive of the important role of hardness in crack propagation resistance of the nanostructured titania coatings.

Adhesion strength of thermal sprayed coatings

The coating made by 20psi of compressed air was also tested according to the ASTM C633 standard test to determine the degree of adhesion or cohesion of a coating to the substrate. The maximum stress that the coating could withstand was measured to be 4829psi which is equal to 33.3MPa. The fracture occurred in the body of the coating, therefore it is impossible to measure the bond strength; on the other hand it is obvious that the bond strength should be greater than the imposed stress in the recent test, which is 33.3 MPa minimum.

This value of adhesion strength for the flame sprayed titania coating is less than the value calculated for the HVOF sprayed nanostructured coating. The calculated value for HVOF sprayed coatings reported when the coating failed at glue was 77 MPa which is twice as large as the calculated value for the flame sprayed counterpart [42]. This difference is probably connected to the larger number of pores and lower concentration of nano-zones present at the flame sprayed coating.

EDX analysis of H₂S testing

To test the ability of the coating to combat corrosive environments, nanostructured coating was put through some simple corrosion tests. Coating made with 20psi of compressed air was placed in a quarts chamber inside an oven and heated to 70° Celsius. A mixture of hydrogen sulfide gas (500ppm) and hydrogen was injected into the chamber and passed over the nanostructured titania coating. The samples were taken out after 5 hours and the polished cross section was sent for microscopy and EDX analysis. The mapping and line scanning results are illustrated at Figs. 29 and 30.
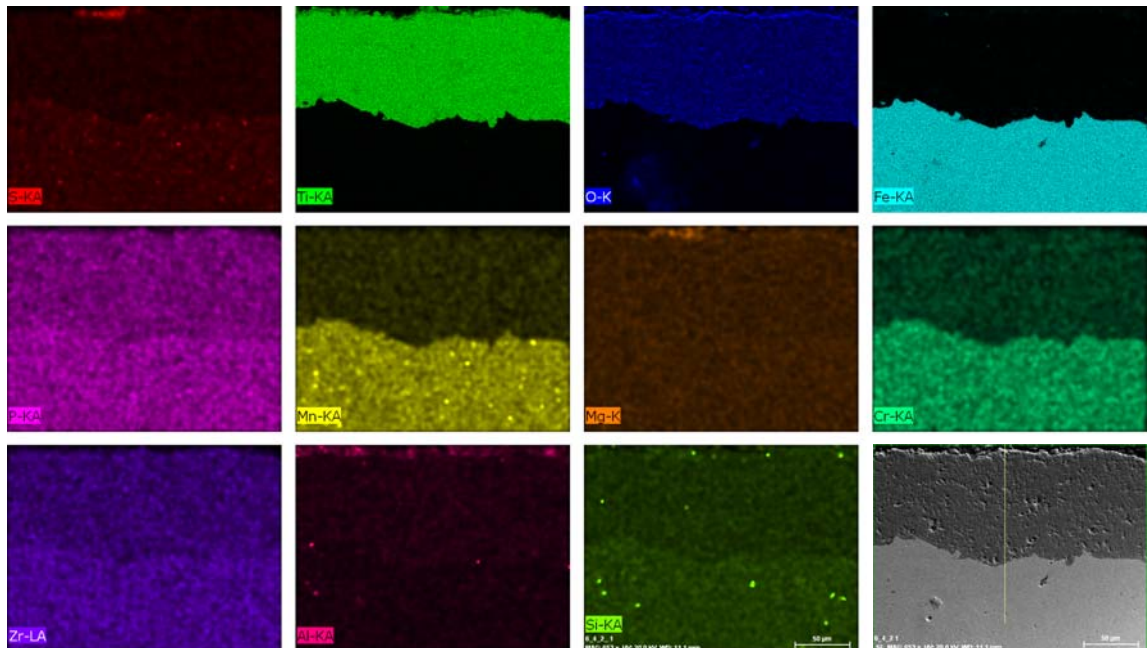
Figure 29: An EDX map of different elements in the coating, the map shows sulfur at the top left corner
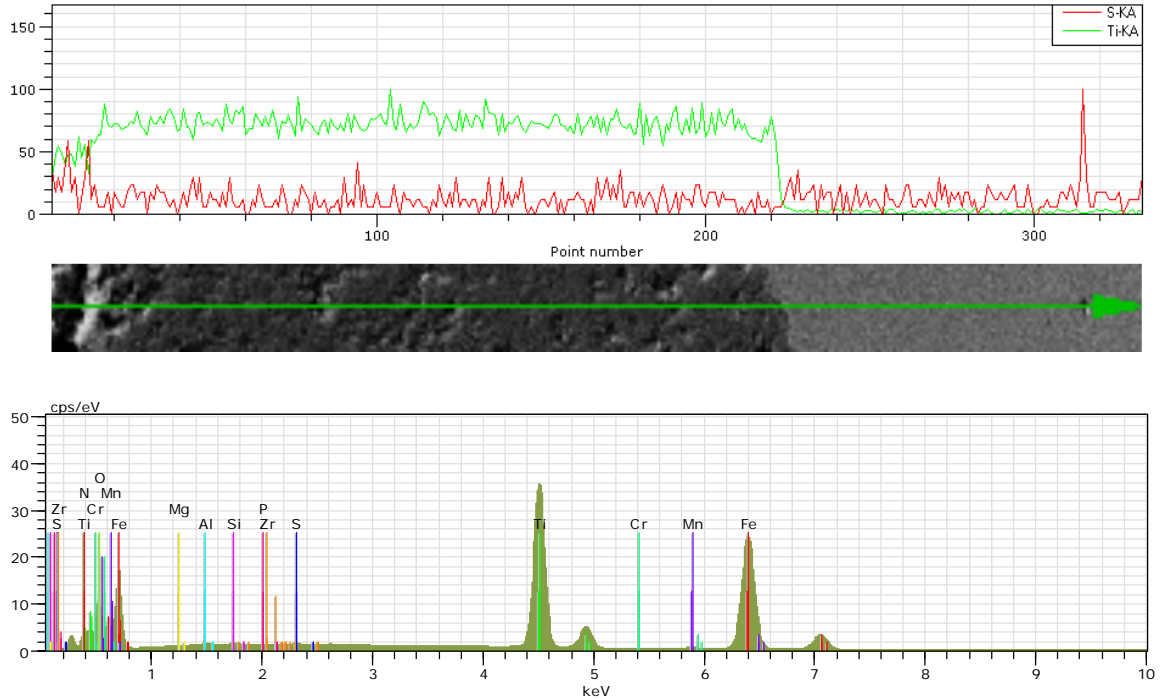
Figure 30: A line scan of the coating which shows traces of sulfur only on the surface

The sulfur diffusion inside the coating is negligible according to the mappings done by EDX. As it is obvious from the sulfur map (red) in Fig. 29 the coating part is the place with the least amount of sulfur content. The red dots visible in the substrate part of the sample are probably the sulfur content of the low carbon steel which has been detected by EDX.

Figure 30 also shows a line scan across the thickness of the coating, which is again suggestive of negligible amount of sulfur diffusion inside of the nanostructured coating. The green line is the content of titanium while the red line shows sulfur which is supposed to be

present in the low carbon steel. Lower porosity of the nanostructured coating can be an advantage in using this sort of coating in places where corrosive chemicals are present.

C hapter 4

Conclusions

Flame sprayed nanostructured and conventional titania coatings were investigated for their mechanical properties and wear resistance. Compressed air was introduced into the flame with various pressures and its effects on the porosity and the hardness of the coatings were studied. The results indicate a lowest porosity and highest hardness levels at approximately 20psi of compressed air pressure. The coating with the best performance was put through ASTM G65 abrasion wear test and the results were quantified using confocal microscopy. The nanostructured coating outperformed the conventional titania and the wear scars on the nanostructured coating was found to be smoother with more plastic deformation. Plowing was found to be the best mechanism to explain nanostructure coatings wear behaviour since less brittle fracture and chipping were observed. The conventional coating showed higher values of average roughness, skewness and

kurtosis, therefore it was concluded that fragmentation, and brittle fracture had an important role in wear mechanism of this type of the coating.

The crack propagation resistance of the nanostructured coating was also been measured and reported in this study. The maximum was observed to happen at approximately 30psi of compressed air pressure. The coating was also been tested for adhesion bonding; although the fracture happened at the body of the coating and not the interface, the results can still be indicative of a minimum adhesion strength of 33.3MPa.

Eventually the coating was subjected to a preliminary H_2S gaseous state corrosion testing; the EDX analysis that has been done on the coating shows no significant trace of sulfur in the nanostructured titania coating. Based on the results presented and the lower cost of flame spraying technique, flame sprayed nanostructured coatings seem to have a better performance than the conventional counterparts when it comes to the wear applications, but they still need more improvements to be able to replace metallic coatings used in industry.

Future work

Despite the low cost and versatility of flame spraying, this thermal spraying technique has not been studied enough by the researchers. Since there are a large number of parameters involved in spraying process, adjusting each of them can open the way to a new mechanical or chemical property improvement which requires more attention. In this regard, finding a method for accurately measuring the nanostructured content of the coatings and quantifying the role of these nanostructured regions in different mechanical properties of titania can be a great achievement toward engineering of nanostructured titania coatings. To this end, finding a way for mathematical modeling of crack propagation in these sorts of materials might be considered as a good approach. Titania coatings can also be considered good chemical resistants. More in-depth corrosion testing of these coatings can also lead to interesting findings which might be helpful for the application of flame sprayed titania coatings in oil and gas industry.

References

[1]   B.A. Kushner and E.R. Novinski, "Thermal Spray Coatings," *ASM Handbook, Volume 18: Friction, Lubrication, and Wear Technology*, ASM International, 2003.

[2]   R. Lima and B. Marple, "Process–property–performance relationships for titanium dioxide coatings engineered from nanostructured and conventional powders," *Materials & Design*, vol. 29, Oct. 2008, pp. 1845-1855.

[3]   K. Bobzin, F. Ernst, K. Richardt, T. Schlaefer, C. Verpoort, and G. Flores, "Thermal spraying of cylinder bores with the Plasma Transferred Wire Arc process," *Surface and Coatings Technology*, vol. 202, Jun. 2008, pp. 4438-4443.

[4]   K. Cooke, G. Oliver, V. Buchanan, and N. Palmer, "Optimisation of the electric wire arc-spraying process for improved wear resistance of

sugar mill roller shells," *Surface and Coatings Technology*, vol. 202, Nov. 2007, pp. 185-188.

[5]   "http://tss.asminternational.org/portal/site/tss/Home/Industries/", ASM International, May 2011.

[6]   "http://www.toledomms.com/Metalizing.htm", Meldrum Mechanical Services, December, 2010.

[7]   "Thermal Spray Materials Guide", Sulzer Metco Inc., issued Feb. 2006, www.sulzermetco.com/en/DesktopDefault.aspx/ tabid-1740//3392_read-5304.

[8]   "Metco 102 Titanium Dioxide powder, technical bulletin, #10-092," Sulzer Metco Inc., issued Oct. 2000.

[9]   J.A. Hawk, R.D. Wilson, D.R. Danks, and M.T. Kiser, "Abrasive Wear Failures," *ASM Handbook, Volume 11: Failure Analysis and Prevention*, 2003.

[10]   R.S. Lima and B.R. Marple, "Thermal Spray Coatings Engineered from Nanostructured Ceramic Agglomerated Powders for Structural, Thermal Barrier and Biomedical Applications: A Review," *Journal of Thermal Spray Technology*, vol. 16, Mar. 2007, pp. 40-63.

[11]   G. Bertrand, C. Meunierb, P. Bertrand, and C. Coddet, "Dried particle plasma spray in-flight synthesis of spinel coatings," *Journal of the European Ceramic Society*, vol. 22, Jun. 2002, pp. 891-902.

[12]   K. Masters, *Spray drying handbook*, Longman scientific and technical.

[13]   D. Goberman, Y. Sohn, L. Shaw, E. Jordan, and M. Gell, "Microstructure development of Al2O3–13wt.%TiO2 plasma sprayed coatings derived from nanocrystalline powders," *Acta Materialia*, vol. 50, Mar. 2002, pp. 1141-1152.

[14]   H. Czichos, M.B. Peterson and W.O. Winer, *Systems Approach to Wear Problems,* 1980, p. 17–34.

[15]   J.D. Gates and G.J. Gore, *Wear of Metals: Philosophies and Practicalities, Mater. Forum, Vol 19,*, 1995.

[16]   K.H. Zum Gahr, *Microstructure and Wear of Materials,* Elsevier Science Publishers, 1987.

[17]   L.T. Kabacoff, "Nanoceramic Coatings Exhibit Much Higher Toughness and Wear Resistance than Conventional Coatings," The AMPTIAC Newsletter, Spring, 2002, 6(1), p 37-42.

[18]   G. Kim and J. Walker, "Successful Application of Nanostructured Titanium Dioxide Coating for High-Pressure Acid-Leach Application," *Journal of Thermal Spray Technology*, vol. 16, Mar. 2007, pp. 34-39.

[19]   H. Luo, D. Goberman, L. Shaw, and M. Gell, "Indentation fracture behavior of plasma-sprayed nanostructured Al2O3–13wt.%TiO2 coatings," *Materials Science and Engineering A*, vol. 346, Apr. 2003, pp. 237-245.

[20] L. Shaw, D. Gobermana , Y. Wang, R. Rena, T. D. Xiao , M. Gella, P. R. Strutt, "The dependency of microstructure and properties of nanostructured coatings on plasma spray conditions," *Surface and Coatings Technology*, vol. 130, Aug. 2000, pp. 1-8.

[21] Y. Wang, S. Jiang, M. Wang, S. Wang, T. Xiao, and P. Strutt, "Abrasive wear characteristics of plasma sprayed nanostructured alumina/titania coatings," *Wear*, vol. 237, Feb. 2000, pp. 176-185.

[22] E. Jordan, M. Gell, Y. Sohn, D. Goberman, L. Shaw, S. Jiang, M. Wang, T. Xiao, Y. Wang, and P. Strutt, "Fabrication and evaluation of plasma sprayed nanostructured alumina–titania coatings with superior properties," *Materials Science and Engineering A*, vol. 301, Mar. 2001, pp. 80-89.

[23] J. Ahn, B. Hwang, E.P. Song, S. Lee, and N.J. Kim, "Correlation of microstructure and wear resistance of Al2O3-TiO2 coatings plasma sprayed with nanopowders," *Metallurgical and Materials Transactions A*, vol. 37, Jun. 2006, pp. 1851-1861.

[24] M. Gell, E. Jordan, Y. Sohn, D. Goberman, L. Shaw, and T. Xiao, "Development and implementation of plasma sprayed nanostructured ceramic coatings," *Surface and Coatings Technology*, vol. 146-147, Oct. 2001, pp. 48-54.

[25] R. Lima, A. Kucuk, and C. Berndt, "Bimodal Distribution of Mechanical Properties on Plasma Sprayed Nanostructured Partially

Stabilized Zirconia," Mater. Sci. Eng. A, Apr. 2002, vol. 327, pp. 224-232.

[26] R. Lima and B. Marple, "Enhanced ductility in thermally sprayed titania coating synthesized using a nanostructured feedstock," *Materials Science and Engineering A*, vol. 395, Mar. 2005, pp. 269-280.

[27] G.E. Kim, J. Walker, Jr., and J.B. Williams, Jr., "Nanostructured Titania Coated Titanium," US Patent 6,835,449 B2, Dec 28, 2004,

[28] R. Lima and B. Marple, "From APS to HVOF spraying of conventional and nanostructured titania feedstock powders: a study on the enhancement of the mechanical properties," *Surface and Coatings Technology*, vol. 200, Mar. 2006, pp. 3428-3437.

[29] X. Lin, Y. Zeng, S.W. Lee, and C. Ding, "Characterization of Alumina-3wt.% Titania Coating Prepared by Plasma Spraying of Nanostructured Powders," *J. Eur. Ceram. Soc.*, Apr. 2004, vol. 24, pp. 627-634.

[30] S. Tao, B. Liang, C. Ding, H. Lao, and C. Coddet, "Wear Characteristics of Plasma Sprayed Nanostructured Yttria Partially Stabilized Zirconia Coatings," *J. Thermal Spray Technol.*, Sept. 2005, vol. 14(4), pp. 518-523.

[31] E. Turunen, T. Varis, T.E. Gustafsson, J. Keskinen, T. Falt, and S.P. Hannula, "Parameter Optimization of HVOF Sprayed Nanostructured

Alumina and Alumina Nickel Composite Coatings," *Surface Coatings Technol.*, Apr. 2006, vol. 200, pp. 4987-4994.

[32]   X. Lin, Y. Zeng, X. Zhou, and C. Ding, "Microstructure of Alumina-3wt.% Titania Coatings by Plasma Spraying with Nanostructured Powders," *Mater. Sci. Eng. A,* Sept. 2003, vol. 357, pp. 228-234.

[33]   D. Goberman, Y. Sohn, L. Shaw, E. Jordan, and M. Gell, "Microstructure development of Al2O3–13wt.%TiO2 plasma sprayed coatings derived from nanocrystalline powders," *Acta Materialia*, vol. 50, Mar. 2002, pp. 1141-1152.

[34]   H. Chen, Y. Zhang, and C. Ding, "Tribological properties of nanostructured zirconia coatings deposited by plasma spraying," *Wear*, vol. 253, Oct. 2002, pp. 885-893.

[35]   H. Chen, C. Ding, P. Zhang, P. La, and S.W. Lee, "Wear of Plasma Sprayed Nanostructured Zirconia Coatings Against Stainless Steel Under Distilled Water Conditions," *Surface Coatings Technol.,* Aug. 2003, vol. 173, pp. 144-149.

[36]   J.F. Li, H. Liao, X.Y. Wang, B. Normand, V. Ji, C.X. Ding, and C. Coddet, "Improvement in Wear Resistance of Plasma Sprayed Yttria Stabilized Zirconia Coating Using Nanostructured Powder," *Tribol. Int.*, Jan. 2004, vol. 37, pp. 77-84.

[37] H. Chen, S. Lee, X. Zheng, and C. Ding, "Evaluation of Unlubricated Wear Properties of Plasma Sprayed Nanostructured and Conventional Zirconia Coatings by SRV Tester," *Wear*, May. 2006, vol. 260, pp. 1053-1060.

[38] G. Bolelli, V. Cannillo, L. Lusvarghi, and T. Manfredini, "Wear behaviour of thermally sprayed ceramic oxide coatings," *Wear*, vol. 261, Dec. 2006, pp. 1298-1315.

[39] N. Berger-Keller, G. Bertrand, C. Filiatre, C. Meunier, and C. Coddet, "Microstructure of plasma-sprayed titania coatings deposited from spray-dried powder," *Surface and Coatings Technology*, vol. 168, May. 2003, pp. 281-290.

[40] M.R. Ranade, a Navrotsky, H.Z. Zhang, J.F. Banfield, S.H. Elder, a Zaban, P.H. Borse, S.K. Kulkarni, G.S. Doran, and H.J. Whitfield, "Energetics of nanocrystalline TiO2.," *Proceedings of the National Academy of Sciences of the United States of America*, vol. 99, Suppl. 2, Apr. 2002, pp. 6476-6481.

[41] M. Stir, R. Nicula, and E. Burkel, "Pressure–temperature phase diagrams of pure and Ag-doped nanocrystalline TiO2 photocatalysts," *Journal of the European Ceramic Society*, vol. 26, 2006, pp. 1547-1553.

[42] M. Gaona, R. Lima, and B. Marple, "Influence of particle temperature and velocity on the microstructure and mechanical behaviour of high velocity oxy-fuel (HVOF)-sprayed nanostructured titania coatings,"

Journal of Materials Processing Technology, vol. 198, Mar. 2008, pp. 426-435.

[43]   ASTM Standard C633, 2008 "Standard Test Method for Adhesion or Cohesion Strength of Thermal Spray Coatings," ASTM International, West Conshohocken, PA, 2008, DOI: 10.1520/C0633-01R08, www.astm.org.

[44]   ASTM Standard C1327- 08 "Standard Test Method for Vickers Indentation Hardness of Advanced Ceramics," ASTM International, West Conshohocken, PA, 2008, DOI: 10.1520/C1327-08, www.astm.org.

[45]   ASTM Standard G65, 2008 "Standard Test Method for Measuring Abrasion Using the Dry Sand / Rubber Wheel," ASTM International, West Conshohocken, PA, 2008, DOI: 10.1520/G0065-04R10, www.astm.org.

[46]   Carl Zeiss GmbH, *Axio CSM 700 Quick Guide*.

[47]   J. Alcala, F. Gauddette, S. Suresh, and S. Sampat, "Instrumented spherical micro-indentation of plasma-sprayed coatings," *Materials Science and Engineering A*, vol. 316, Nov. 2001, pp. 1-10.

[48]   P. Ctibor, P. Bohac, M. Stranyanek, and R. Ctvrtlik, "Structure and mechanical properties of plasma sprayed coatings of titania and alumina," *Journal of the European Ceramic Society*, vol. 26, 2006, pp. 3509-3514.

[49] X. Liu, B. Zhang, and Z. Deng, "Grinding of nanostructured ceramic coatings: surface observations and material removal mechanisms," *International Journal of Machine Tools and Manufacture*, vol. 42, Dec. 2002, pp. 1665-1676.

[50] S. Malkin and T. W. Hwang, "Grinding Mechanisms for Ceramics," *CIRP Annals - Manufacturing Technology*, vol. 45, 1996, pp. 569-580.

[51] B.S. Chang, C.K. Lee, K.S. Hong, H.J. Youn, H.S. Ryu, S.S. Chung, and K.W. Park, "Osteoconduction at porous hydroxyapatite with various pore configurations.," *Biomaterials*, vol. 21, Jun. 2000, pp. 1291-8.

[52] P.S. Eggli, W. Muller, and R.K. Schenk, "Porous hydroxyapatite and tricalcium phosphate cylinders with two different pore size ranges implanted in the cancellous bone of rabbits. A comparative histomorphometric and histologic study of bony ingrowth and implant substitution," *Clin. Orthop. Relat. Res*, vol. 232, 1998, pp. 127–138.

[53] Y. Okazaki, E. Gotoh, T. Manabe, and K. Kobayashi, "Comparison of metal concentrations in rat tibia tissues with various metallic implants.," *Biomaterials*, vol. 25, Dec. 2004, pp. 5913-20.

[54] J. Pawley, ed., *Handbook of Biological Confocal Microscopy (3rd ed.)*, Berlin, Springer, 2006.

[55] A. McDonald, M. Lamontagne, S. Chandra, and C. Moreau, "Photographing Impact of Plasma-Sprayed Particles on Metal

Substrates," *Journal of Thermal Spray Technology*, vol. 15, Dec. 2006, pp. 708-716.

[56] R. Lima, S. Kruger, and B. Marple, "Towards engineering isotropic behaviour of mechanical properties in thermally sprayed ceramic coatings," *Surface and Coatings Technology*, vol. 202, Apr. 2008, pp. 3643-3652.

[57] B. Jeffery, M. Peppler, R.S. Lima, and a McDonald, "Bactericidal Effects of HVOF-Sprayed Nanostructured TiO2 on Pseudomonas aeruginosa," *Journal of Thermal Spray Technology*, vol. 19, Aug. 2009, pp. 344-349.

[58] S. Bakardjieva, J. Subrt, V. Stengl, M. Dianez, and M. Sayagues, "Photoactivity of anatase–rutile TiO nanocrystalline mixtures obtained by heat treatment of homogeneously precipitated anatase," *Applied Catalysis B: Environmental*, vol. 58, Jun. 2005, pp. 193-202.

[59] G. Anstis, P. Chantikul, B.R. Lawn, and D. Marshall, "A critical evaluation of indentation techniques for measuring fracture toughness: I, direct crack measurements," *Journal of the American Ceramic Society*, vol. 64, 1981, pp. 533–538.